Chapter 10
Toward a Predictive Hierarchical Multiscale Modeling Approach for Energetic Materials

Brian C. Barnes, John K. Brennan, Edward F. C. Byrd, Sergei Izvekov, James P. Larentzos and Betsy M. Rice

Abstract This chapter describes efforts to enable multiscale modeling of energetic material response to insult through a concurrent hierarchical multiscale framework. As a demonstration, a quantum-derived, particle-based coarse-grain model of an energetic material is used to provide part of the constitutive response in a finite element multiphysics simulation. Bottom-up coarse-grain models of hexahydro-1,3,5-trinitro-*s*-triazine (RDX) and the methods used to perform reactive simulations at the microscale will be described. Simulations demonstrating microstructure-dependent initiation are also presented. Research opportunities addressing the remaining challenges related to detonation are discussed.

Keywords Hierarchical multiscale modeling · Energetic materials · Dissipative particle dynamics · Bottom-up coarse-grain models · Condensed phase chemistry · Quantum mechanics

10.1 Introduction

A grand challenge for modeling and simulation (M&S) of the properties and response of energetic materials (EM) is virtual assessment of EM performance in munitions, providing a substantial time and monetary savings in the development of materials for next-generation weapons. Current M&S capabilities have numerous shortfalls that do not yet allow accurate, predictive in silico assessment, or even reliable suc-

B. C. Barnes · J. K. Brennan · E. F. C. Byrd · S. Izvekov · J. P. Larentzos · B. M. Rice (✉)
US Army Research Laboratory, Aberdeen, USA
e-mail: betsy.rice.civ@mail.mil

© Springer Nature Switzerland AG 2019

N. Goldman (ed.), *Computational Approaches for Chemistry Under Extreme Conditions*, Challenges and Advances in Computational Chemistry and Physics 28,
https://doi.org/10.1007/978-3-030-05600-1_10

cess in virtual design or screening of new EM. These include a lack of micro- and mesoscale modeling capabilities necessary to represent salient physical and chemical features of the materials, deficiencies in multidisciplinary linkages of the relevant scales, and the existence of high levels of empiricism in continuum simulations. Furthermore, the inaccuracy and uncertainty in the descriptions of energetic material response at the microscale and beyond are problematic, especially in the treatment of chemical reactivity. In light of these shortfalls, vigorous research efforts have been pursued by us and others [1–8] to develop simulation capabilities to adequately capture microstructural dependencies on macroscopic events—a simulation challenge for many materials [9–16] and inherent to the initiation of EMs [17].

Our efforts in this area focus on the development of a multiscale M&S framework to predict EM response when subjected to thermal or mechanical insults. While particle-based and continuum level simulation methodologies and models have been extensively studied and advanced [18, 19], the coupling of grain-scale, nonequilibrium microstructural changes between the microscale and macroscale is not commonly realized due in part to methodological challenges [20] in multiscale modeling, as well as computational limitations of mesoscale modeling. As an illustration, consider the case of plate impact on either a single-crystal or formulated energetic material. Classical molecular simulations of one-dimensional (1D) impact under boundary conditions of uniaxial strain typically involve 10^4–10^7 particles (reaching up to micron length scales in one dimension) for durations reaching hundreds of picoseconds. However, experimental setups may be measured in centimeters or larger, in all dimensions, while observations occur over microseconds. Direct molecular simulation of these macroscale systems is simply unfeasible. Current engineering or continuum models used by most in the EM community are parameterized against macroscale experimental data for particular materials, where any atomistic or mesoscale mechanisms affecting material response are implicitly present, as opposed to naturally emerging via models that represent microstructural features as statistical distributions or material history variables. Reaction models used at the continuum level, whether based on matching a specific set of experiments or analysis of atomistic simulations, rarely incorporate explicit dependencies of the reaction chemistry on evolving microstructure, particularly under extreme temperatures and pressures. Furthermore, the role of initial reaction chemistry in changing mechanical constitutive behavior for the interactions of materials at the grain level is not typically utilized in continuum models.

For these reasons, some of our recent efforts have been focused on advancing the nascent microscale models/methods and scale-bridging approaches required for the multiscale M&S framework. Our overall long-term goals have been to develop the appropriate models and approaches that will overcome these gaps, leading to a predictive capability to simulate the coupled thermophysical, chemical and mechanical material processes that affect material response. Within this chapter, we will describe our efforts to properly depict microstructural features in continuum simulations of EM via a multiscale hierarchical approach that bridges higher resolution modeling and the continuum.

We will first describe the higher resolution model and method development at the coarse-grain (CG) level that enables particle-based reactive simulations at the microscale. Particle-based microscale simulation methods utilizing CG models currently offer a promising route for extending atomistic modeling toward the microscale with a significant gain in computational efficiency. CG models, generated by grouping a set of smaller entities (e.g., atoms or molecules) into a single larger entity, are built in a *bottom-up* fashion, such that they incorporate the key underlying physics from the higher resolution scale. During this coarse-graining process, the reduction in molecular degrees-of-freedom (d.o.f.) provides a gain in computational efficiency; however, the loss of information must be adequately recovered through the CG methodology. Furthermore, at the atomistic scale, the formation and breaking of chemical bonds is treated explicitly, while at the microscale, the CG models and methods must collectively capture and recover the relevant chemical features lost during coarse-graining.

We will then discuss our efforts to understand condensed phase chemistry under extreme temperature and pressure, and provide perspectives regarding realistic chemistry that is to be included into a CG model that treats chemical reactivity. This will be followed by an overview of multiscale approaches for continuum simulations that make use of information from particle-based simulations, including our chosen approach, a concurrent hierarchical multiscale simulation method (HMS) that couples continuum and particle-based CG simulations. Finally, we will describe our scale-bridging and algorithmic research efforts within HMS, including the use of machine learning to increase computational efficiency, and provide demonstrations of the HMS approach using our CG models and methods. The chapter will conclude with a discussion of new research opportunities and future directions.

10.2 Coarse-Grain Models

Simulation of the complete range of EM responses, including the competing mechanisms of energy flow, mass flow, and chemical reactivity, requires modeling at length and timescales that are far beyond those amenable to atomistic-scale approaches. Quantum chemical approaches based on ab initio, density functional theory (DFT) or semiempirical calculations can provide detailed information about chemical reactions and transition state structures, but tend to be limited in the number of atoms that can be treated; thus, they are unable to capture the full extent of heterogeneity present in real microstructured materials. Classical reactive potentials that describe the energy landscape and barriers between initial material, the reaction products, and the relevant transition states are available [21], for example, ReaxFF [22, 23] is a commonly employed atomistic force field for modeling EMs. All-atom reactive molecular dynamics (MD) simulations of EMs have been applied to examine the initiation and growth of hot spots created near a single microstructural heterogeneity [24], when the material is subjected to thermal and mechanical loading. However, these simulations of an isolated, nanometer-sized heterogeneity still required

petascale computational resources. As such, the computational expense quickly becomes impractical, requiring years of wall clock time when attempting to simulate realistic samples containing a collection of microscale heterogeneities. These well-recognized limitations of modeling at the atomistic scale provided the motivation for the work described here: the development of microscale models and methods to bridge these spatial and temporal modeling regimes while ensuring multiscale consistency. Until recently, the requisite microscale computational capabilities were either nonexistent or lacking. In this section, we will describe our efforts in developing tools for building CG models, while our efforts in developing the necessary CG methodologies will be described in the following section.

Discrete particle-like descriptions for computationally feasible modeling of EM at the microscale can be obtained through two distinct approaches. One is derived from macroscale data and governing equations (discretization of continuum models), which has demonstrated success in going beyond simple homogeneous systems, but still remains within an essentially macroscopic phenomenological framework, thereby severely limiting its predictive capability [25]. The second approach, which we will discuss in detail, is bottom-up particle-based coarse-graining, in which groups of atoms are mapped into a statistically equivalent ensemble of structure-less CG particles interacting via CG force fields derived from microscopic information [26–29].

In this approach, the atomistic coordinate space is reduced to a smaller space of CG coordinates commonly associated with center-of-mass (CoM) coordinates of molecular clusters representing the CG particles, while the CG dynamics is considered to be Newtonian. Considerable efforts have been expended in the search for CG conservative force fields that lead to a correct representation of equilibrium atomistic statistics and, hence, correct thermodynamics of the CG ensemble [30]. Among the growing efforts to develop conservative force fields for CG models, of particular interest for the work presented here were efforts to generalize CG models for fluids with complicated EOS. These efforts resulted in the development of many-body interaction models [31–33]. Conservative forces in such models can be viewed as effective (mean) forces, where these forces arise due to changes in a many-body potential of mean force (PMF). Approximations to the CG PMF energy surface can be obtained from microscopic data with a number of bottom-up methods such as structure inversion [34], force-matching [35–41], or entropy-matching approaches [42].

One efficient technique for producing well-performing bottom-up approximations to the CG PMF is the multiscale coarse-graining (MS-CG) method [35–38, 43–50]. The MS-CG method has been described elsewhere [36, 40, 41, 51] as a parameter-free force-matching approach that yields an optimal pairwise decomposition of CG conservative forces, and therefore of the associated CG PMF. Consequently, the MS-CG approach is our method of choice for parameterization of the CG models for EM. The MS-CG method can be naturally extended to include a dependence on thermodynamic state variables such as density or temperature, which further enhances the transferability of the CG models [39, 41, 52]. This is important for simulations of shocked EM, where an exceptionally broad spectrum of thermodynamic conditions ranging from ambient to extreme temperatures and pressures may be sampled.

For realistic molecular environments found in condensed-matter systems such as EM, however, the CG conservative models typically fail to yield correct time correlations of the CG dynamical variables leading to accelerated dynamics and affecting the corresponding transport properties. This failure has been attributed to the absence of interparticle friction and thermal noise in the CG description, both of which lead to energy dissipation due to the coupling to the atomistic intraparticle (irrelevant) dynamics with the surroundings. Consequently, bottom-up modeling of both thermodynamic and transport properties require thermodynamically consistent modeling of both the CG conservative (PMF) and nonconservative (dissipative) interactions.

In developing a bottom-up description of the CG nonconservative interactions, we have capitalized on recent advances in formulating the CG dynamics from first principles [51, 53–55]. In these works, the CG equations of motion in the form of generalized Langevin equations (GLE) have been derived from the microscopic Newtonian equations by means of the Mori-Zwanzig formalism. The Mori-Zwanzig formalism leads to the thermodynamically consistent decomposition of the microscopic forces into CG conservative and nonconservative contributions. Within the pairwise and Markovian limits, which are always valid for systems interacting with nonlinear potentials at sufficiently aggressive coarse-graining, the GLE dynamics acquires a classical Galilean invariant form of the Dissipative Particle Dynamics (DPD) [56, 57] equations with the conservative forces precisely prescribed by the MS-CG approach. Initially, the DPD equations were introduced phenomenologically to describe the hydrodynamics of simple liquids using a particle-based approach. The derivation of the DPD equations from first principles in this fashion provides one with a recipe to parameterize the CG models in a fully bottom-up fashion and has led to new systematic approaches to extract the distance-dependent radial and shear dissipative and random forces directly from the atomistic data [51, 58–60]. Our recently proposed multiscale methodology [51, 60] to extract nonconservative interactions from atomistic interactions and dynamics data complements the MS-CG approach to provide a robust framework for bottom-up parameterization of both the conservative and nonconservative forces used in the DPD methodology.

In the following sections, we briefly review the basics of the approaches for first principles parameterization of the conservative and nonconservative force fields for use in the DPD equations of motion and then discuss their applications to two well-studied energetic materials, hexahydro-1,3,5-trinitro-*s*-triazine (RDX, $C_3H_6N_6O_6$) and nitromethane (NM, CH_3NO_2).

10.2.1 Conservative DPD Force Fields

10.2.1.1 The MS-CG Method

The MS-CG method is described [35–37, 40, 47, 51] as a force-matching-based approach for constructing a least-squares optimal pairwise decomposition of a (conservative) force field $\left(F_I^C\right)$ and corresponding many-body CG PMF $\left(W^{\mathrm{PMF}}\right)$. In the

MS-CG approach, the intrinsic many-body force F_I^C is approximated by a pairwise and central force field $F_I^{C,2b}$. The latter force field is determined using a database of the microscopic forces F_I associated with the CG coordinates R_I by minimizing the merit function

$$\chi^2(\alpha) = \left\langle \frac{1}{N}\sum_{I=1}^{N}\left|F_I - F_I^{C,2b}(\alpha)\right|^2 + \left|3VP^{\text{atm}} - 3Nk_BT^{\text{atm}} - \sum_{I=1}^{N} F_I^{C,2b}(\alpha)\cdot R_I\right|^2 \right\rangle \quad (10.1)$$

with respect to spline parameters α used to represent each pair term in the $F_I^{C,2b}$. In the atomistic system, the CG coordinates R_I are located at the CoM of an atomic group mapped into a CG particle. The optional pressure constraint introduced by the second term in (10.1), where T^{atm} and P^{atm} are, respectively, the atomistic temperature and pressure, leads to a CG model suitable for *NPT* simulations [36, 39, 45].

One approach to account for, on average, the many-body interactions within the two-body representation is to use pair terms $f^C(R_{IJ}, \rho)$ in $F_I^{C,2b}(\alpha)$ that are functions of a particle number density distribution, ρ, and where R_{IJ} is the interparticle distance [39, 41, 52]. This density dependency is not merely an abstract construction, but realistically describes the EOS-dependent interactions at the CG scale. As matter of fact, the force-matching expressed by (10.1) yields a different force $f^C(R, \rho, T)$ at each thermodynamic state point (e.g., density ρ and temperature T), when applied to the atomistic system at different state points. In general, both the density ρ and temperature T dependency are needed to ensure a correct EOS for the CG system.

For a homogeneous, single component system, the particle density could be defined based on the global density $\rho \equiv \langle\rho\rangle = N/V$, while alternatively, the notion of a local particle density $\rho(R_I)$ associated with the Ith particle could also be implemented. In the latter approach, the PMF remains a regular function of particle position, and therefore, this approach avoids the issues that otherwise plague global density-dependent interactions [61]. A local particle density definition is more appropriate for systems whose local structure may dramatically vary, such as a microstructured material under thermal or mechanical loading. A consistent approach for defining $\rho(R_I)$ from a discrete set of masses is to use weight functions centered on particles $\rho(R_I) = \sum_{J\neq I}\omega_\rho(R_{IJ})$, where the density weight function $\omega_\rho(R_{IJ})$ has compact support [52]. Neglecting the explicit temperature dependency of $f^C(R_{IJ}, \rho, T)$, an assumption that often is justified, the density dependency can be introduced numerically via interpolation of $f^C(R_{IJ}, \rho)$ to a set of forces $\left\{f^C(R_{IJ}, \rho^s)\right\}$ calculated for a reference system at a set of specific thermodynamic densities $\{\rho^s\}$. Although linear interpolation is considered to be adequate [39, 41] in most DPD applications, it leads to unacceptable energy conservation in the energy-conserving DPD method (DPD-E), described hereafter. A computationally efficient density dependency that results in an exactly integrable force field (and hence better energy conservation) can be written as [52, 62]

$$f^C(R_{IJ}, \rho_I, \rho_J) = f_0^C(R_{IJ}) + \frac{1}{2}\omega_D(R_{IJ})[A(\rho_I) + A(\rho_J)] \quad (10.2)$$

where $f_0^C(R) = f^C\left(R, \rho^0\right)$ is the MS-CG pair term for the density ρ^0 at ambient conditions, $\omega_D(R)$ is a preselected distance weighting function, and $A(\rho)$ is chosen to generate the desired EOS. Integrating the density-dependent MS-CG force field with pair terms given by (10.2) results in the pairwise decomposition of the CG PMF into a sum of potentials $w^{\mathrm{PMF}}(R_{IJ}, \rho)$.

10.2.1.2 Application to RDX and NM: Parameterization of Conservative MS-CG Models

The MS-CG methodology has been applied to derive accurate and transferrable CG conservative force fields for RDX [41, 52, 63] and NM [39, 51, 60]. The mapping of the atomistic RDX and NM structure into a one-bead CG representation is displayed in Fig. 10.1a. The performance of the MS-CG approach for aggressive coarse-graining where clusters of many molecules mapped into a CG particle was explored for liquid NM and proved to be successful [60]. Specifically, a hierarchy of MS-CG models starting with one NM molecule per Voronoi cell (Fig. 10.1a) and up to 64 NM molecules per cell (Fig. 10.1b) was able to accurately describe the structure and density of the atomistic liquid NM under constant *NPT* conditions.

Calculated MS-CG potential terms $w^{\mathrm{PMF}}(R, \rho)$ for different pressures (densities) for the density-dependent MS-CG models of RDX and NM are shown in Fig. 10.2 [39, 41, 52]. The density dependency for the NM model was introduced through linear interpolation of MS-CG potentials for different densities. For RDX, the model with local density dependency using the representation in (10.2) (referred to as the

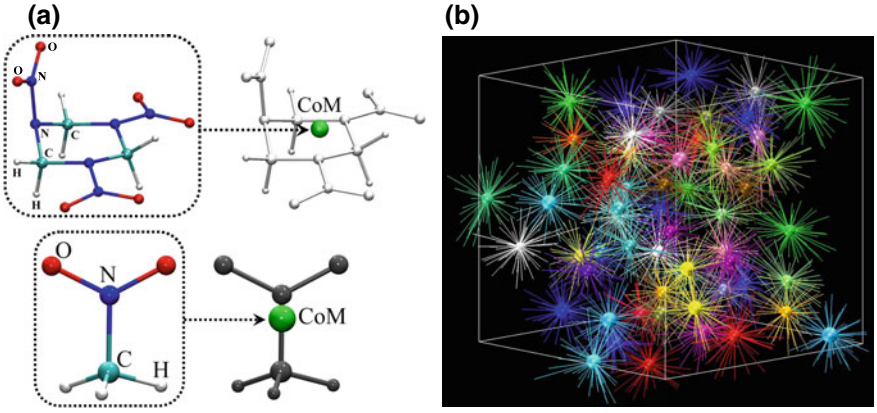

Fig. 10.1 Panel **a**: Mapping of RDX (top) and NM (bottom) into a one-site representation. Panel **b**: Visualization of partitioning of liquid NM (3840 molecules) into centroidal Voronoi cells with 64 molecules per cell. The large balls represent CoMs (centroids) of the Voronoi cells, while the lines shown connect the Voronoi cell centroids to the molecular CoM that are associated with the cell. Colors are used to visually delineate individual clusters (reprinted from Izvekov, S.; Rice, B. M., *J. Chem. Phys.* **2014,** *140* (10), 104104, with the permission of AIP Publishing)

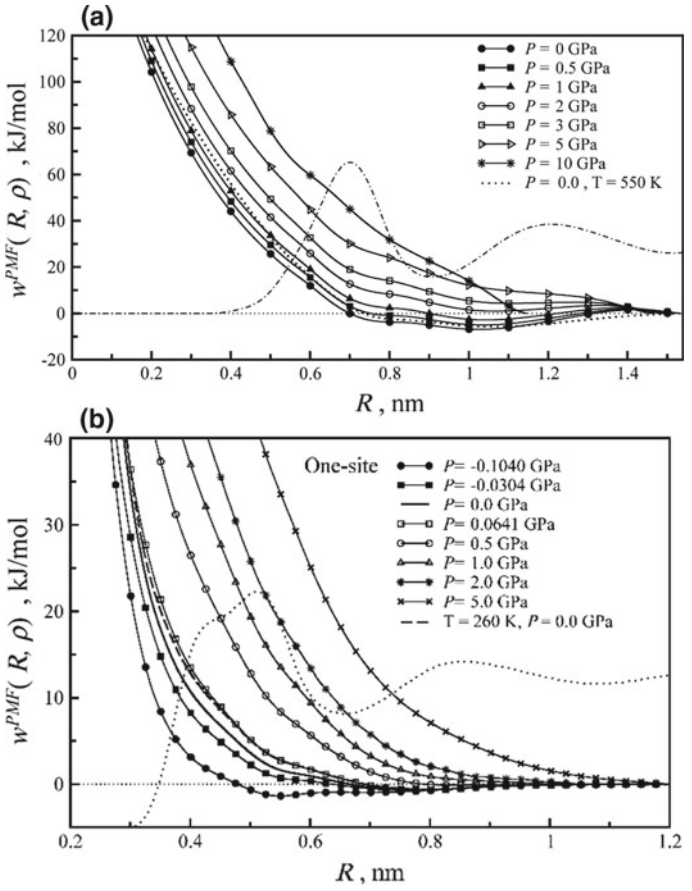

Fig. 10.2 One-site density-dependent MS-CG models of RDX (Panel **a**) and NM (Panel **b**). The scaled CoM RDFs are shown by the dot-dashed and dotted lines (Reprinted from (a) Izvekov, S.; Chung, P. W.; Rice, B. M., *J. Chem. Phys.* **2011,** *135* (4), 044112 and (b) Izvekov, S.; Chung, P. W.; Rice, B. M., *J. Chem. Phys.* **2010,** *133* (6), 064109, with the permission of AIP Publishing.)

MS-CG-D(E) model) was introduced to achieve the energy conservation required for DPD-E simulations of RDX [52].

Due to the systematic representation of microscopic interactions, the MS-CG conservative models describe the equilibrium properties of these explosives reasonably well under different thermodynamic conditions and in different phases. In particular, the MS-CG model of RDX well describes various material properties, including the structure of the ideal RDX crystal [52]. A summary of key thermodynamic and mechanical properties for crystalline RDX from (i) experiment, (ii) atomistic simulations using the reference atomistic force field of Smith and Bharadwaj (the SB model) [64], and (iii) MD simulations of the MS-CG model at ambient pressure is given in Table 10.1.

Table 10.1 Lattice constants a, b, c, density ρ, volumetric thermal expansion coefficient α_V, isothermal bulk modulus B_T, and atmospheric melting temperature T_{melt} of crystalline RDX, from experiment, the atomistic reference and the MS-CG model

Property	Experiment	Atomistic	MS-CG[a]
a (Å)	13.18[b]	13.45[c]	13.37
b (Å)	11.57[b]	11.53[c]	11.58
c (Å)	10.71[b]	10.53[c]	10.59
ρ (kg/m^3)	1806[b]	1805[c]	1801
α_V (10^{-5} 1/K)	19.34[d]	16.38[c], 10.94[e]	8.32
B_T (GPa)	12.1[f], 11.99[g]	13.0[c]	13.17
T_{melt} (K)	478.6[h]	488.5[i]	468.8

[a]Moore et al. [52]
[b]Choi and Prince [65] 300 K
[c]Munday et al. [66] 300 K
[d]Cady [67]
[e]Podeszwza et al. [68]
[f]Olinger et al. [69] 293 K
[g]Haycraft [70] 295 K
[h]Hall [71]
[i]Sellers et al. [72]

The elastic stiffness constants C_{ij} are compared in Table 10.2 to the results for the reference atomistic model, density functional theory (DFT) calculations, and to experiment. The table also reports Cauchy pressures for an MS-CG model crystal, which are measures of the deviation from purely two-body interactions. A similar or better level of agreement is achieved for MS-CG models of NM [39].

Introducing density dependency into the MS-CG potentials leads to significantly improved mechanical properties of the materials under elevated pressures. This is particularly challenging due to the well-known problem of representability, i.e., at a given state point, no single pair potential may exist that can capture all the properties of a given material [61]. The exceptional transferability of the MS-CG models make them suitable for application to systems under thermal and mechanical loading [75]. The level of accuracy and transferability achieved with the MS-CG approach would be difficult to reproduce using the conventional top-down approaches [29, 76, 77].

10.2.2 Nonconservative DPD Force Fields

10.2.2.1 Multiscale Coarse-Graining of Nonconservative Interactions

A characteristic feature of the DPD methodology is the dissipative force that acts between particles, which provides a means of depicting the atomistic model dynamics with a CG model. We have refined the standard dissipative contributions and incorpo-

Table 10.2 Stiffness constants C_{ij} for the MS-CG model of crystalline RDX compared to experimental, ab initio, and empirical atomistic model data

C_{ij} (GPa)	Experiment[d,e]	ab initio[c]	Atomistic[a,b]	MS-CG[a]
C_{11}	36.67[d], 25.02[e]	29.96	30.64[a], 25.00[b]	21.03
C_{12}	1.38, 8.21	7.48	12.68, 10.60	10.06
C_{13}	1.67, 5.81	4.52	7.92, 7.60	11.49
C_{22}	25.67, 19.60	25.51	29.41, 23.80	20.98
C_{23}	9.17, 5.90	5.28	10.64, 8.80	11.50
C_{33}	21.64, 17.93	23.61	30.23, 23.40	23.53
C_{44}	11.99, 5.17	5.34	4.16, 3.10	6.11
C_{55}	2.72, 4.07	4.83	6.54, 5.20	6.10
C_{66}	7.68, 6.91	8.59	10.03, 7.70	5.23
C_{13}–C_{14}	N/A	N/A	N/A	5.38
C_{12}–C_{66}	N/A	N/A	N/A	4.83

[a]Moore et al. [52] 0 K
[b]Munday et al. [66] 300 K
[c]Taylor [73] 0 K, DFT-D3
[d]Haycraft [70] 295 K
[e]Haussuhl [74] 293 K

rated them into the DPD-RX framework, including multidirectional dissipative interactions [78, 79] that are both parallel and perpendicular to the interparticle separation axis. Directional dissipative force contributions attempt to capture the CG d.o.f. that contribute to the molecular shape or polarity. The multiscale bottom-up approach to derive the radial (parallel) $\left[\gamma^{||}(R)\right]$ and shear (perpendicular) $\left[\gamma^{\perp}(R)\right]$ friction functions dependent on the interparticle separation R is proposed and described in detail elsewhere [60]. The friction functions $\gamma^{||}(R)$ and $\gamma^{\perp}(R)$ describe the amplitudes of the nonconservative force components that are parallel and perpendicular to the interparticle separation, respectively. The approach exploits the statistical independence of the random forces and the initial particle velocities, which is a generic property of the GLE dynamics, and hence the DPD method. This property allows a unique relationship between the friction functions, and both the three-body velocity–velocity correlation functions $c^{\alpha\beta}_{VV}$, $\alpha, \beta \in \{||, \perp\}$ and the two-body correlation functions $\left[c^{\alpha}_{\Delta FV}\right]$ of residual force, $\Delta F_I = F_I - F^C_I$, with velocity. By introducing the mesh $\{R_l, l = 1, \ldots, N_{\text{bin}}\}$ of interparticle distances and considering the correlation functions at a sufficiently large moment of time T_M, the orthogonality relation leads to the following linear system of equations

$$\sum_{\tilde{l}=1}^{N_{\text{bin}}} \left[c^{\alpha||}_{VV}(T_M, R_l, R_{\tilde{l}})\gamma^{||}(R_{\tilde{l}}) + c^{\alpha\perp}_{VV}(T_M, R_l, R_{\tilde{l}})\gamma^{\perp}(R_{\tilde{l}})\right] = -c^{\alpha}_{\Delta FV}(T_M, R_l), \alpha = ||, \perp \quad (10.3)$$

Equation (10.3) allows the friction functions $\gamma^{||}(R)$, $\gamma^{\perp}(R)$ to be uniquely determined on the distance mesh. The friction functions are thermodynamically consistent with the MS-CG conservative force used to compute the correlation functions $c^{\alpha}_{\Delta FV}$. Following the standard DPD formalism, the random forces for both the parallel and perpendicular contributions are modeled a priori with fluctuation–dissipation theorem-compliant white noise (uncorrelated in time). The appropriate fluctuation–dissipation relations for both the parallel and perpendicular contributions can be found elsewhere [75].

10.2.2.2 Application to RDX and NM: Parameterization of Nonconservative Forces

The accurate description of transport phenomena, such as diffusion and viscosity, with the DPD approach, requires the parameterization of radial, $\gamma^{||}(R)$, and shear, $\gamma^{\perp}(R)$, friction functions. The application of the multiscale methodology presented in Sect. 10.2.2.1 for RDX [63] and NM [51, 60] leads to accurate $\gamma^{||}(R)$ and $\gamma^{\perp}(R)$ friction functions that are thermodynamically consistent with the conservative interactions (Fig. 10.3). The radial friction function $\gamma^{||}(R)$ for NM was found to exhibit a typical form at fine coarse-graining [51, 60]. In contrast to this and to bottom-up nonconservative DPD forces of real molecular liquids discussed in the literature, the dissipative dynamics of RDX is dominated by the shear friction $\gamma^{\perp}(R)$, and hence cannot be accurately simulated using standard DPD, which accounts for only the radial friction $\gamma^{||}(R)$. The analysis of DPD simulations using MS-CG forces for RDX highlights the importance of the perpendicular friction on the short-time dynamics and transport properties. Evidently, the way in which the dissipation in molten RDX is partitioned (with the shear component being dominant) is a result of concerted translational and intramolecular conformational dynamics of the RDX molecules. Therefore, the RDX dissipation dynamics is distinctly different from those observed in liquid NM and other molecular liquids [41, 51], which are well described by nonconservative DPD forces with dominant radial friction. We note in the DPD methods described below, both shear and radial friction terms have been included.

10.2.3 Outlook

Our future efforts are directed toward formulating novel extensions of the MS-CG method to create a hierarchy of high-fidelity bottom-up CG models for explosive formulations. We intend to create CG particle interactions (potentials) that are dependent upon other aspects of the particle's local environment beyond local density, such as the three-body local arrangement or more complex order parameters. We also intend to incorporate a wide range of multibody interactions as well as dipolar and higher order electronic polarizability interactions that are pertinent to EM composites. For

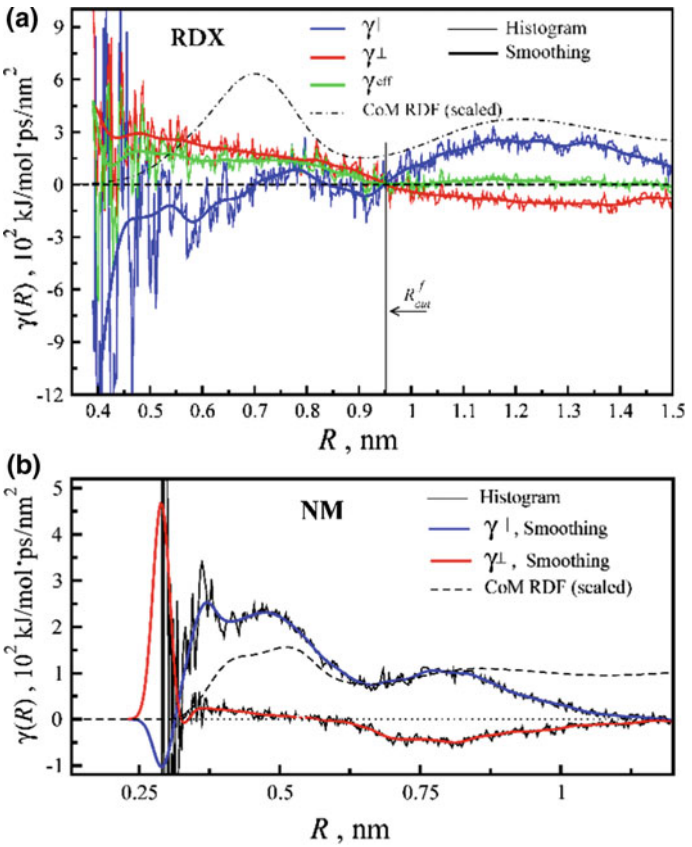

Fig. 10.3 Histogram data (thin noisy) and Gaussian filter smoothing [51, 63] (thick) of friction functions $\gamma^{||}(R)$, $\gamma^{\perp}(R)$ for the one-site MS-CG models of RDX (Panel **a**) and NM (Panel **b**) obtained by solving (10.3). The scaled CoM radial distribution functions (RDFs) are shown by dot-dashed lines. For the MS-CG-D(E) model for RDX, the vertical line and arrow show the choice of cutoff distance $\left(R_{\text{cut}}^{f}\right)$ for the frictions, and $\gamma^{\text{eff}}(R)$ is the effective friction [34]. (From Izvekov, S.; Rice, B. M., *Phys. Chem. Chem. Phys.* **2015**, *17* (16), 10795–804.)

example, we believe that noncentral three-body interactions might play an important role in the microstructure evolution of EMs under shock, particularly in the molecular level plastic response, while the dipolar and higher order electronic polarizability interactions have longer range effects that will influence the structural response at longer scales. In order to have thermodynamically consistent capabilities to model the microscale, however, coarse-grained models cannot be generated separately from the development of the methods that use them, since features lost during the required process of coarse-graining will not be adequately recovered unless reintroduced in some fashion, namely the simulation method. Thus, we now turn our attention to the DPD-based methodologies used to simulate solid EM under a range of threats.

10.3 Coarse-Grain Methods

Computationally reasonable particle-based simulations of material behavior governed by micro- and mesoscale structural heterogeneities require the development of CG models such as those just described. However, careful consideration must be taken for the choice of not only a CG *model*, but as critically, for the choice of an appropriate CG *methodology*, especially since the use of their results in higher scale simulations will strongly influence the outcome. To determine properties other than static (equilibrium) properties, the CG-molecular dynamics (CG-MD) approach is not adequate due to the well-known speedup of the dynamics of CG models compared to their atomistic model counterparts, which is a direct consequence of losing d.o.f. during coarse-graining [80, 81]. Moreover, at the atomistic scale, the formation and breaking of chemical bonds is treated explicitly and is conceptually intuitive, but at the microscale, the CG models and methods must collectively capture and recover the relevant physics and chemistry lost during coarse-graining.

The development of CG modeling methods is an active field, where most of the attention has been given to treating the static behavior of *soft matter* (see e.g., [82, 83]). These systems are amenable to coarse-graining because some atomic motions (e.g., hydrogen vibrations) contribute minimally to the backbone behavior and resulting equilibrated microstructure. Further, the weakly repulsive interaction potentials for such systems allow on the order of 10^{-13} s time steps to be used, providing access to phenomena that occur on microsecond timescales. However, only a relatively limited number of CG model studies have attempted to reproduce nonequilibrium behavior [84–92], in part due to the challenge of mapping the CG and atomistic model dynamics. Thus, we have made significant investments in CG methods development to describe nonequilibrium behavior.

An overview of our efforts described here has entailed creating computational capabilities targeting the microscale that allow for physically realistic simulations of the thermomechanical response of EM composites with microstructure. Particle-based microscale simulation methods utilizing CG models currently offer a promising route into and beyond the microscale, the critical time and spatial regime that cannot be accessed with atomistic MD. We have chosen microscale methods that are built upon the DPD method [56, 57], a technique initially developed for the simulation of soft matter, but recently applied to condensed phase matter [75, 92]. Our microscale approach, which incorporates the salient physics, couples CG models with reactive microscale methods, where both are described within this chapter. These efforts are designed to provide predictive capabilities that are amenable to direct coupling with continuum level models in a multiscale modeling framework, or to provide crucial information for development of higher fidelity continuum material models. The direct coupling efforts are described in Sect. 10.5.

10.3.1 CG Method: Variants of DPD

10.3.1.1 General Description

The DPD method is now a well-established CG particle simulation method that has evolved substantially since its inception in 1992 [56, 57]. Advances in both method and model development now allow DPD simulation of a wide range of material classes from soft matter, such as polymers and biomolecules, to condensed matter, such as metals and crystals [52, 89, 93]. DPD is well grounded in statistical mechanics and stochastic dynamics, allowing for a physics-based interpretation of the parameters and their determination from higher resolution models. Advances in the method continually arise from work in various material communities, further extending its potential applicability and utility.

The original formulation of the DPD method conserves total momentum only and thus is limited to modeling isothermal processes. For the purpose of simulating EM composite response, the energy-conserving DPD method (DPD-E) [92, 94–96] is particularly critical since it enables nonequilibrium simulation scenarios and thermally variant conditions. DPD-E uniquely treats the CG d.o.f. through both the dissipative forces and a particle internal energy term. The particle internal energy term plays two roles within the DPD-E method. First, it provides a numerical means of ensuring energy conservation during the simulation. Moreover, the particle internal energy term provides an additional mechanism to recover the coarse-grain d.o.f., which is essential for accurately reproducing the atomistic model behavior [75].

Building upon the ideas of Maillet and co-workers [86, 91], we recently developed a general DPD framework that incorporates chemical reactivity (DPD-RX) [75]. Originally constructed for DPD-E, the DPD-RX method can be formulated upon either this variant or the constant-enthalpy DPD variant (DPD-H) [92], notated as DPD-RX-E and DPD-RX-H, respectively. In either variant, a reaction progress variable is assigned to each particle that monitors the time evolution of an *extent-of-reaction* associated with each of the prescribed reactions that may occur within each particle. As such, the DPD-RX approach does not necessitate a reactive potential that involves explicit bond breaking and bond forming. The chemical reactivity can be modeled using complex or reduced reaction mechanisms and allows for both unimolecular and multimolecular collision reactions to be simulated via both direct and indirect approaches. Aside from including the extent-of-reaction and introducing an additional term to the particle internal energy (u_{chem}), the DPD-E and DPD-H formalisms do not change. In practice, for every time step, DPD-RX dynamics are separated into three elementary, physical processes: (1) *inert dynamics*—execution of the DPD-E (or DPD-H) equations of motion; (2) *CG-reactor chemistry*—extent-of-reaction change within each CG particle based upon the prescribed chemistry; and (3) *reaction energy update*—partitioning of the chemical energy release or gain by updating the CG particle internal energy, during which the total energy of the given CG particle does not change. As the chemistry of a CG particle changes, so

does its interaction potential. The interaction potential changes in such a way that it captures both heat exchange and pressure–volume work due to chemical reactivity.

10.3.1.2 Equations of Motion

In the DPD-E method, at any time t, a particle I is specified by its mass m_I, position $\mathbf{r}_I$, momentum $\mathbf{p}_I$, and internal energy u_I. The particle internal energy accounts for the energy absorbed or released by the d.o.f of the higher resolution model that are unresolved as a result of coarse-graining; u_I is coupled to the internal temperature θ_I through a CG equation of state (CG-EOS) typically defined as, $u_I = u_I(\theta_I)$. The variation of the internal energy $\mathrm{d}u_I$ can be written as the sum of contributions that correspond to the mechanical work done on the system, $\mathrm{d}u_I^{\mathrm{mech}}$, and the heat conduction between particles, $\mathrm{d}u_I^{\mathrm{cond}}$, i.e., $\mathrm{d}u_I = \mathrm{d}u_I^{\mathrm{mech}} + \mathrm{d}u_I^{\mathrm{cond}}$. In DPD-E, two types of temperatures are defined, a kinetic temperature, T_{kin}, which is associated with the external d.o.f., and the internal temperature, θ_I, which is associated with the internal d.o.f. At equilibrium conditions, these two temperatures will be statistically equivalent, but not necessarily under nonequilibrium conditions.

Extending the DPD-E method to the reactive case requires the variance of the particle internal energy $\mathrm{d}u_I$ to include an additional contribution that corresponds to the energy associated with changes in chemistry, $\mathrm{d}u_I^{\mathrm{chem}}$. The total variance is given by $\mathrm{d}u_I = \mathrm{d}u_I^{\mathrm{mech}} + \mathrm{d}u_I^{\mathrm{cond}} + \mathrm{d}u_I^{\mathrm{chem}}$, where the total energy of the system is assumed to remain constant during changes in $\mathrm{d}u_I^{\mathrm{chem}}$. The set of equations of motion for DPD-E is accompanied by an update of u_I^{chem} specified as

$$\mathrm{d}u_I^{\mathrm{chem}} = -\mathrm{d}u_I^{\mathrm{CG}} \quad (I = 1, \ldots, N) \tag{10.4}$$

where u_I^{CG} is the CG interaction energy of particle I. Equation (10.4) follows from the requirement of total system energy conservation, such that the total energy of each particle is assumed to be conserved upon any concentration change due to the reaction. Analogous to the nonreactive DPD-E approaches, conservation of the total momentum and the total system energy, $E = U^{\mathrm{CG}} + K + \sum_I u_I$, is satisfied, where $K = \sum_I \frac{\mathbf{p}_I \cdot \mathbf{p}_I}{2m_I}$ is the total kinetic energy and U^{CG} is the total CG interaction energy. For the DPD-RX approach presented here, any change in the CG particle chemistry is also reflected through a species-dependent CG-EOS, $u_I = u_I\left(\theta_I, N_\xi\right)$, where N_ξ is the number of molecular species ξ in the product gas mixture. The choice of $u_I\left(\theta_I, N_\xi\right)$ is a modeling decision, where a possible formulation is to consider the isolated molecule contributions based upon the molar heat of formation, $\Delta H_{f,\xi}(T_r)$, and the isobaric heat capacity of each molecular species $C^0_{P,\xi}(\theta_I)$, taken at some reference state [75]. The development of alternative formulations is an ongoing pursuit by our group.

10.3.1.3 Reaction Model

The DPD-RX framework presented here builds upon the treatment of the CG particles seemingly as interacting continuous-stirred tank reactors [97] or *CG-reactors*. The CG-reactor depicts temporal changes in the species type and concentration of the molecules representing the CG particle, where these changes in chemistry are governed by the prescribed set of reaction mechanisms and kinetics, termed the *reaction model*. For further illustration of the DPD-RX methodology, consider a specific reaction model, namely, the thermal decomposition of crystalline RDX into a mixture of product gases. From global reaction rate models of high-temperature combustion of nitramines, a reduced reaction mechanism was determined, where the resulting RDX decomposition pathway is a four-step reaction rate model [75] consisting of a unimolecular, irreversible reaction:

$$\mathrm{RDX} \rightarrow 3\mathrm{HCN} + \frac{3}{2}(\mathrm{NO_2} + \mathrm{NO} + \mathrm{H_2O}) \tag{10.5}$$

and three bimolecular, irreversible reactions:

$$\begin{aligned} \mathrm{HCN} + \mathrm{NO_2} &\rightarrow \mathrm{NO} + \frac{1}{2}(\mathrm{N_2} + \mathrm{H_2}) + \mathrm{CO} \\ \mathrm{HCN} + \mathrm{NO} &\rightarrow \mathrm{CO} + \mathrm{N_2} + \frac{1}{2}\mathrm{H_2} \\ \mathrm{NO} + \mathrm{CO} &\rightarrow \frac{1}{2}\mathrm{N_2} + \mathrm{CO_2} \end{aligned} \tag{10.6}$$

Each reaction rate constant is modeled by a standard temperature-dependent Arrhenius expression, where the temperature used is a local weight-average internal temperature of CG particle I, defined as

$$\bar{\theta}_I^{-1} = \frac{\sum_{J=1} \omega_{\mathrm{Lucy}}(r_{IJ})\, \theta_J^{-1}}{\sum_{J=1} \omega_{\mathrm{Lucy}}(r_{IJ})} \tag{10.7}$$

where J includes the neighboring particles of I and itself, and $\omega_{\mathrm{Lucy}}(r_{IJ})$ is the Lucy function [98]. A local-average particle internal temperature used in the reaction rate expressions implicitly depicts multimolecular conditions and the local environment of a chemically reacting mixture. Nevertheless, the forms of $\overline{\theta_I}$ and ω_{Lucy} are modeling choices, where alternative forms are possible. Further discussion of the choice of the reaction model specifically for EM simulations is given below in Sect. 10.4.

10.3.1.4 Particle Model

In the DPD-RX method, the particle interaction potential is not a reactive type potential that mimics chemistry through bond breaking and subsequent formation of tran-

sition structures and reaction products (e.g., [23, 99]). Rather, the evolving chemistry modeled by the CG-reactor depiction is directly coupled to the interaction potential of the CG particle. In the application presented here, the chemical character of any particle can vary between two end states, unreacted RDX and a final product gas mixture, with many continuous chemical states in between. An RDX molecule is represented by the isotropic one-site CG model (CG-RDX) [52] obtained by the MS-CG method described above, while the product gas mixture is modeled using the exponential-six interaction potential [100]. A notable feature of this model is that the expansion of hot product gases is inherently captured through the chemistry-dependent particle interactions via changes in the particle excluded volumes.

10.3.1.5 Practical Aspects

Beyond attempting to reproduce the correct physics, the development and implementation of the CG framework requires several practical considerations. A plethora of numerical integration schemes have been extensively explored (e.g., [85, 92, 101–106]), allowing for stable, accurate, and efficient simulations. Recently our group has adopted an efficient integration scheme for the DPD variants based on the Shardlow-splitting algorithm (SSA) [92, 104, 107]. Compared to the traditional DPD integrators, the SSA allows for larger time steps, on the order of 10^3, making simulations of CG models of EM composites possible for the DPD-E and DPD-H variants. Advancements to the DPD methods and algorithms are continually incorporated within the highly-scalable open-source LAMMPS (Large-scale Atomic/Molecular Massively Parallel Simulator) simulation package [108] to provide a long-term, sustainable modeling framework that can readily leverage high-performance computing resources. Such practical considerations are critical for enabling simulations with 10^7–10^9 particles at the relevant time and length scales for EM composite models.

10.3.2 Sample Applications

The DPD variants can be applied to gain a fundamental understanding of the energetic material response to shock. Consider the shock profiles of the CG-RDX model with those of a nonreactive atomistic model [64] at conditions under which reactions are not expected to occur (see Fig. 10.4). Clearly, the MD simulation of the CG-RDX model significantly overpredicts the thermal response, due to improperly accounting for the energy and momentum exchange. This leads to a kinetic temperature increase that is significantly higher than the atomistic model temperature at and behind the shock front. In the DPD-E simulation, the transfer of mechanical energy from the plate impact into the CG d.o.f. has appropriately occurred via the heat and momentum exchange between the particle internal energies. In the CG-MD simulation, the particles behave effectively as hard spheres, while the DPD-E simulation allows for

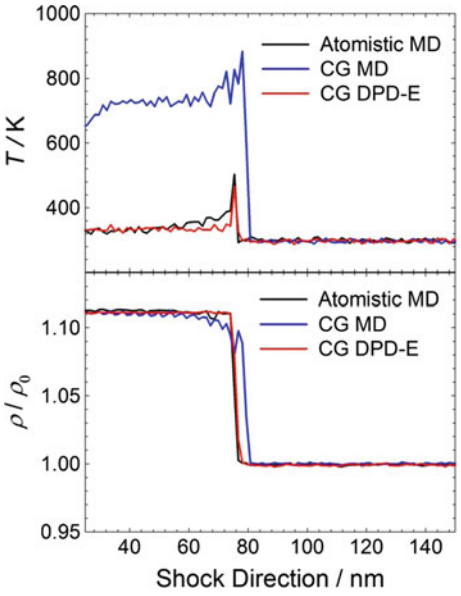

Fig. 10.4 Comparison of the nonequilibrium, nonreactive response of pure crystalline RDX: (atomistic MD) fully atomistic model using MD; (CG-MD) one-site CG-RDX model using MD; and (CG DPD-E) due to mechanical shock generated by plate impact at $u_p = 0.5\,\mathrm{km/s}$. Kinetic temperature and density profiles are snapshots taken 15.0 ps after impact (Adapted with permission from Brennan et al., *J. Phys. Chem. Lett.*, **2014**, *5* (12), pp 2144–2149. Copyright 2014 American Chemical Society.)

some of the momentum exchange to be absorbed into the particle internal energies via the CG-EOS.

Next, consider applications of the DPD-RX-E method to examine the effects of microstructural heterogeneities on the material response to mechanical shock. Variations in the local geometry and density may lead to significantly different hotspot formation, which dictates the macroscopic material response. In the examples below, several microstructures are generated to examine the role that defects and complex grain boundaries play in the material response. In the first scenario, 10-nm spherical inclusions are randomly distributed throughout the 2.5 μm sample. The sample is slammed into a reflective wall in the −z-direction, generating a shock compression wave that propagates through the sample in the +z-direction. As the shock front passes through the material, the spherical inclusions collapse, transferring mechanical energy to heat the particles and initiating chemical reactions. The particle internal temperature and reaction progress (defined as the fraction of RDX that is present in the particle) is shown in Fig. 10.5, where after approximately 0.5 ns, the shock front reaches the end of the 2.5 μm sample. In cases with sufficiently large shock velocities and/or defect sizes, the spherical inclusions are observed to combine and coalesce into larger reaction zones.

To examine the effects of grain boundaries on material response, a polycrystalline RDX microstructure geometry is constructed using a Voronoi tessellation method, where the polyhedra are treated as individual grains (Fig. 10.6a). The particle-based model of each grain is subsequently grown as a perfect crystal that is free of any intragranular defects. The resulting structure is a large polycrystalline network of randomly oriented HCP-like ordered grains with complex, planar interfaces and inter-

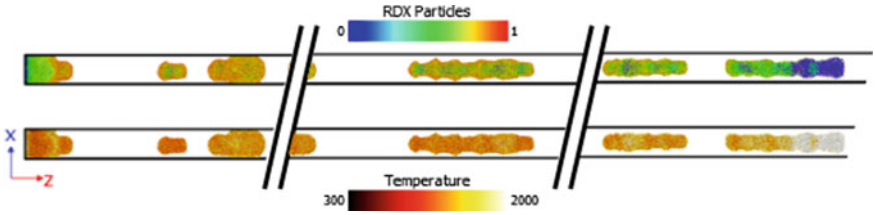

Fig. 10.5 Snapshots along the sample for the reaction progress (top) and particle internal temperature (bottom) at various positions along the z-axis of a 2.5 μm shocked RDX sample. The initial, unshocked sample included a random distribution of 10-nm spherical inclusions that collapse, creating localized hot spots that initiate chemistry. The unreacted material in the sample is not shown for visual clarity and to depict the surface area of the reaction zones

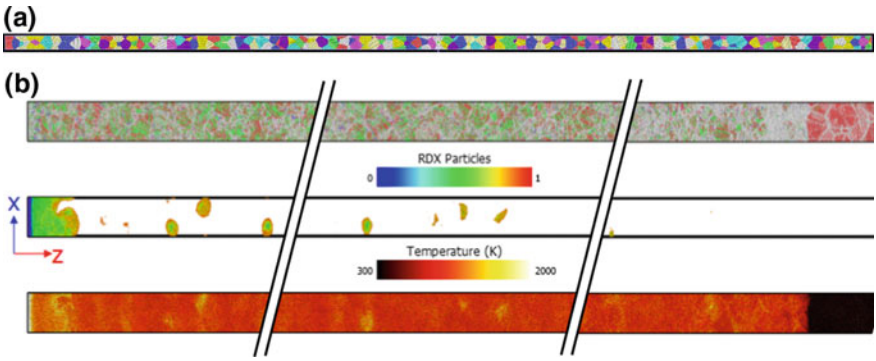

Fig. 10.6 **a** The initial, unshocked polycrystalline RDX sample. **b** Snapshots along the sample for the common neighbor analysis (top), reaction progress (middle), and internal temperature (bottom) at various positions along the z-axis of the 2.5 μm sample. For the reaction progress snapshots, the unreacted material in the sample is not shown for visual clarity and to depict the surface area of the reaction zones. The common neighbor analysis uses the following coloring scheme: HCP = pink, FCC = Green, BCC = Blue, ICO = Yellow, and White = Other

granular voids. As the material undergoes shock compression, a common neighbor analysis is performed to highlight the initial, unshocked HCP-like grains and the resulting microstructure that evolves due to shock (see Fig. 10.6b). These particle-based methods are able to capture the microstructural heterogeneities and short-time physics that evolve immediately after the shock wave passes through the sample, enabling the exploration and understanding of the fundamental mechanisms that influence material performance. In this particular microstructure, energy localizes at the inter-granular voids, creating localized hot spots where chemical reactions begin to evolve. The behavior of the void collapse differs from the previous microstructure due to the varying volume sizes, shapes, and locations.

10.3.3 Outlook

For the goal of understanding EM composite performance, we developed a CG method framework that allows us to begin exploring the role of explicit microstructural heterogeneities in these materials. While numerous atomic-scale reactive potentials are available within the literature (e.g., [23, 99, 109]) that also allow the exploration of the effects of microstructure, they are limited to studies of single, isolated defects due to computational cost [110]. CG approaches such as those presented here allow exploration into previously unattainable temporal scales. Given that the time step in a particle simulation is dictated by the highest frequency modes, which are coarsened away in a CG model, time steps that are thousands of times larger may be taken [92, 104]. Application of CG models and methods that treat chemical reactivity extend the length and timescales well beyond those currently realizable in atomistic simulations, enabling exploration of microstructure-dependent material systems that was not previously possible.

While the DPD-RX framework enables simulations at vastly different length and timescales as compared to atomistic-scale simulations, the computational speedup comes at the cost of losing atomistic detail. By design, the CG model behavior cannot replicate the total fidelity of the atomistic model behavior. Rather, the intent is for the CG model simulation to produce results of sufficient accuracy across a broad range of material properties and behavior for the problem of interest, but for considerably less computational expense. In other words, efforts are made to strike a balance between maintaining the d.o.f. that reproduce the key atomistic model behavior, while decreasing the overall computational cost. To this end, we continue to optimize the recovery of the salient d.o.f. through improvements and refinements of the CG model development and the DPD-RX framework. Several possible refinements and future research directions for the DPD-RX framework are highlighted next.

The particle interaction model for the product gas mixture (pgm) is a first-generation model, where an assortment of modifications for extending the transferability of the model to describe a wider range of chemical states typically present under the extreme conditions of shock and thermal loading is needed. In determining the interaction potential for the pgm model, significant effort is required to adequately sample the reacting environment in a statistically reliable manner, which is dependent upon both the density and species concentrations. Simulation data from finer-scale models, as well as an analytical EOS for the exponential-6 potential may reduce some of the burdens. Furthermore, to minimize the limitations of the single-site exponential-6 interaction potential currently being used for the pgm model, the development of a density-dependent model is under consideration.

Some further refinements that would make the method framework more generally applicable are possible. For example, the DPD-RX framework can be extended to permit intra- as well as interparticle reactions, i.e., reactions influenced by the composition and temperature of either the particles themselves solely, or also the surrounding particles, respectively. The intraparticle approach implicitly accounts for mass diffusion of the reacting species, which under certain circumstances (e.g.,

short timescales) may be sufficient to accurately represent the salient behavior, but in other scenarios, mass diffusion may play a key role. The interparticle approach more directly mimics multimolecule reactions, where explicit treatment of mass diffusion can occur via species transfer between CG particles. Further work is underway to extend the DPD-RX framework to allow other variations of reactions, including non-bond breaking reactions such as molecular conformational transitions [111].

Finally, specific to understanding the reactive behavior of EMs under extreme conditions, improvements to the reaction model itself are needed. Currently, the four-step reduced kinetics model for RDX decomposition described above is used, where this reaction model exhibits density-dependence consistent with the condensed phase. Moreover, the DPD-RX framework ensures that the chemical energy content from the reaction model, starting with pure RDX and ending with product gases, is thermodynamically consistent through the use of standard state data taken from either thermochemical data tables or ab initio calculations. Simulation studies using the current reaction model are expected to provide reliable qualitative trends, as a means of mapping the relative roles of various types of microstructure heterogeneity in EM composites. Nonetheless, much is unknown about the condensed phase chemistry of EM, so uncertainty remains regarding the accuracy of our particular reduced reaction model. Hence, more investigation and development is needed to provide the most accurate depiction of the condensed phase chemistry. The DPD-RX framework is sufficiently general such that it allows any (practical) number and type of reactions and the associated species to be implemented, including pressure-dependent reaction models. Therefore, if new insight gained from higher resolution simulation techniques, such as those described in the next section, or novel experiments lead to the development of more accurate reaction models, then these models can be readily implemented.

10.4 Condensed Phase Chemistry Under Extreme Conditions

10.4.1 Development of Reaction Models for DPD-RX

A description of the chemical reactivity is needed to complete our approach to model the microscale response. As indicated above, this description must be amenable for use at the CG scale within the DPD-RX methodology. In this CG representation, the description of the interparticle interactions is dependent on the CG material state whether unreacted, partially reacted, or fully reacted. As described earlier, the current DPD-RX methodology assumes each CG particle behaves as a well-stirred reactor [75], whose chemical composition is governed during the simulation by a corresponding extent-of-reaction variable for each reaction in a prescribed chemical kinetics mechanism. In its current form, the DPD-RX method requires a description of the chemical composition of the CG-reactor during the decomposition of the

solid EM to gaseous products, which in turn is dependent on the chemical kinetics mechanism.

Derivations of full chemical kinetics mechanisms based on elementary reactions [112] and subsequent reduction to computationally tractable reduced-order chemical kinetics models (ROM) are conceptually straightforward and have been very successful when used in numerous applications including combustion modeling [113]. The DPD-RX methodology demonstrated above for shock loading of the CG-RDX model uses such a reduced four-step chemical kinetics model [75], which was based on gas-phase reaction mechanisms for nitramine combustion [114] combined with a single-step rate of RDX decomposition above the melting temperature [115]. However, while this chemical kinetics model qualitatively exhibits the expected behavior, it may not properly represent the actual condensed phase reactivity in extreme nonequilibrium conditions, such as those associated with high-pressure, high-temperature shock states (>10 GPa and >1000 K). The material environment in these highly dense conditions (>2.0 g/cm^3) allows for different chemistries that would not be accessible at less extreme conditions. Thus, because a reaction model is required in the DPD-RX framework, it is necessary to obtain an accurate microscale description of the extent of chemical reaction of an energetic material subjected to insult, whether a detonation or a sub-detonative response (often even more challenging to model) is the final result. Some of the challenges that exist for transitioning the condensed phase chemistry behavior into the DPD-RX framework will be considered at the end of this section. However, prior to that, we will describe the challenges in first determining just the reaction mechanism for chemistry occurring under these extreme conditions, where consideration for determining the associated kinetics are left for discussion elsewhere.

10.4.2 Scope of the Problem and Challenges

As chemical reactions are inherently atomistic processes, the proper simulation methodology to obtain rate information is through atomistic approaches, preferably using accurate quantum mechanical (QM) methods. QM methods applied to the systems at hand, are typically limited to simulations of a few picoseconds using <10^5 atoms. Numerous classical and quantum-mechanically based MD simulations of thermally and mechanically initiated energetic materials have been published [116–153], some of which attempt to describe reaction rates and mechanisms of the material in extreme conditions. However, as nicely detailed in a review by Manaa and Fried [117], determination of accurate rate information from atomistic simulations of energetic materials in highly nonequilibrium high-density states is a daunting undertaking. The most obvious challenges pertain to the complexity of the event, spawning several questions that must be considered: Is it possible to unravel the complex dependence of concurrent reactive processes occurring in a heterogeneously dense environment under extremely nonequilibrium conditions into a series of individual reaction steps? Does the simulation adequately sample the phase space for a suf-

ficiently long time to observe all important reactions? Is all relevant phase space represented in the simulation? Is the level of theory adequate to properly describe the material state under these extreme conditions? Do computational tricks imposed for simulation efficiency [18] introduce artifacts that might influence outcomes?

Provided these questions can be adequately addressed, there are additional concerns as to whether chemical species can be properly identified for monitoring throughout a simulation, the most direct manner in which to determine the extent of reaction. Using empirical classical reactive models, assignment of bonds can be readily accomplished, thus allowing for monitoring species evolution throughout a trajectory. However, there is always the question whether the material states, which might be far from those of the training set used to parameterize the empirical model, are properly described. Thus, a more predictive, less empirical quantum-based level of theory is appropriate for use in these simulations. This leads to questions about the adequacy of the QM method. At what conditions do approximations in the chosen QM theory [116] break down? Furthermore, within a QM representation, there is no unique way to define electron localization and therefore, no unique way of defining whether atom pairs are bonded, or whether species are radicals or ions. For example, species may be identified based on bond distance and lifetime criteria, a reasonable, but nonunique scheme to determine chemical moieties [117]. However, different sets of bond distance and lifetime criteria could result in different sets of observed chemical moieties. Without a unique means of identifying species, individual reaction steps, the key to the classical chemical kinetics mechanisms, cannot unambiguously be determined and monitored to measure lifetimes.

Perhaps the single most difficult challenge is accurately simulating the overall event. Current computational capabilities allow for certain QM methods (e.g., DFT) to simulate systems under extreme conditions, thus reducing reliance on empirical models but at an increased computational expense. It would be desirable to use highly accurate QM methods, such as the "gold standard" of QM (coupled cluster with singles, double, and perturbative triples excitations [CCSD(T)]) [116]; however, this method is extremely computational intensive and is limited to approximately 20–40 atoms for a single time step. Outside of this consideration of accuracy versus computation time, the simulations suffer from several other deficiencies that might introduce error into the results. First, the systems being simulated are highly idealized, and a realistic material environment is inadequately described. The computational requirements for QM simulations of this type preclude inclusion of material heterogeneities in the simulation cell and do not allow for simulations of processes that go beyond a few picoseconds (assuming system sizes no larger than 10^5 atoms). For some simulations, selection of appropriate initial conditions is tricky and fraught with opportunity to introduce bias. For example, in quantum molecular dynamics (QMD) simulations that target a specific thermodynamic state at an extreme temperature and/or pressure (such as Wu et al. [154] and Rice and Byrd [155]), equilibrating the system might result in chemical reactions occurring before the desired thermodynamic state is reached. This, in turn, could influence subsequent chemistry once the targeted thermodynamic state is reached. Thus, it must be considered whether the initial state and subsequent equilibration protocol had biased the resulting chemistry as the desired

thermodynamic state was approached. Rice and Byrd attempted to address these issues by performing two isothermal–isobaric QMD simulations of formic acid at extreme conditions in which chemistry was observed, and for which the initial conditions were dramatically different [155]. In these two simulations, densities and potential energies converged to the same values on the time scale of the simulations. This information was used to predict a shock Hugoniot point using assumed final thermodynamic states. However, due to the limited simulation time, it could not be determined whether full chemical equilibrium was reached, thus potentially influencing the predicted shock Hugoniot point. Furthermore, in simulations of this kind, the equations of motion are coupled to a thermostat and/or barostat, which could influence chemical reactions as energy is adjusted to achieve the desired temperature and pressure. For example, the dissipation rate of thermal energy originating from exothermic reactions will depend on a thermostat's damping parameter.

Simulations other than those that target-specific thermodynamic states, such as the aforementioned examples [154, 155], are also susceptible to potential errors by virtue of their simulation protocol or process. For example, in some simulations to explore onset of thermal decomposition [117, 126, 130, 131, 140, 142, 151, 156], a system is first optimized or equilibrated to a state in which reaction does not occur and is then heated, leading to the question of how the heating rate is influencing the chemistry, and whether the heating rate is realistic. For shock simulations, two approaches are used to explore shock-initiated chemistry: direct mechanical shock simulation or the multiscale shock technique (MSST) [157, 158]. For the former approach, of which there are multiple schemes available for mechanically generating a shocked sample, the system is often overdriven in order to observe chemical reaction within a computationally feasible time frame. The question is raised as to whether the chemistry resulting from the overdriven shock (leading to a higher degree of material compression) is relevant to the chemistry associated with steady-state detonation or that initiated by a weaker shock. On the other hand, while several studies [118, 119, 121–124, 132, 133, 135, 136, 145] have been used to explore the chemistry resulting from a shock using the MSST approach (which allows for smaller simulation sizes, and thus longer times), the inherent assumptions within MSST regarding stress gradients and thermal gradients limit its accuracy in describing material states immediately behind the shock front. Thus, it is unlikely that direct mechanical shock and MSST simulations would yield the same initial chemistries directly behind the shock front. This, in turn, could influence subsequent chemistry across the reaction zone. An example limitation of MSST is that it does not explicitly model a wave traveling through the sample. As such, some aspects of anisotropic material response cannot be captured, as microstructural features (e.g., voids, grain boundaries) will not experience a directional shock wave moving through them. Another advantage of MSST over direct shock simulation is that it allows for the convenient inclusion of quantum nuclear effects [159, 160], which may decrease the shock strength necessary to observe the onset of reactions. For both MSST and direct mechanical shock simulations, it is possible that the chemistry is biased due to the initial conditions, equilibration protocol, and simulation process.

Furthermore, these nonequilibrium simulations are performed within the constraints of periodic boundary conditions, which can be problematic if the material's thermodynamic properties or local structure becomes significantly inhomogeneous within the simulation cell (such as conditions under mechanical loading). These local variances (which may further increase with reaction during the simulation) could interact with the periodic images and adversely influence the outcome. Some of these errors are introduced because of system size and time limitations; they can be somewhat mitigated by using empirical or semiempirical approaches, such as reactive force fields [22, 23] or tight-binding DFT (DFTB) [161] to perform substantially larger and longer simulations [117]. However, the accuracy of these methods cannot be assumed for conditions beyond those used for parameterization.

Even when using DFT, the accuracy of the methods at extreme conditions is a limiting factor. As opposed to gas-phase processes, the highly accurate multi-reference QM approaches used in the evaluation of elementary reaction rates cannot be applied to the condensed phase, due to computational costs. (For a further discussion of quantum mechanical methods, see Taylor and Rice [116]). Additionally, at extreme conditions, electronic excited states might play a role in chemistry; these could not be treated by single-reference DFT. Furthermore, pseudopotentials used for computational efficiency might introduce errors for highly compressed material. However, as DFT is the most reasonably accurate ab initio approach available to predict reactions in a shocked condensed phase system at this time [116, 117], we consider it the best approach to model chemistry of an energetic material under extreme conditions, and thus, DFT is being used in our attempts to determine a condensed phase reaction model for use in DPD-RX.

10.4.3 Some Illustrations of the Challenges

An illustration of some of the difficulties associated with DFT simulations described above is evident in a heroic study by Wu and co-workers [154], in which they attempted to examine the chemistry of solid PETN compressed to the estimated Chapman–Jouguet (CJ) density of 2.38 g/cm^3 and heated to temperatures of 3,000 and 4,200 K (the estimated CJ temperature) using DFT isothermal–isochoric (NVT) simulations. By "painstakingly" tracking reactions during the simulations, Wu et al. found, for example, "over 3,000 unique reactions, 78% of which only occur once in the simulation" in a periodic simulation cell containing only four molecules [154]. With computational platforms and algorithms substantially improved since the 2009 Wu et al. study [154] that allow for system sizes and simulation times of 10^5 atoms and picosecond timescales, respectively, using DFT, the complexity and number of the reactions discovered are expected to increase. Wu et al. were able to determine that material conversion under these conditions involved catalysis by water and its decomposition products, a distinctly different process than those assumed in more traditional proposed decomposition mechanisms [154]. The catalytic process is possible due to the extreme conditions, in which water rapidly dissociates and provides

a continual source of OH and H. By virtue of this ease of dissociation, Wu et al. suggest that "bonds containing hydrogen are inherently nonmolecular, and thus the CJ state should not be treated as a mixture of conventional molecules" [154].

Likewise, our own forays into large-scale QM studies of materials under shock conditions have shown us that unusual chemistries can occur. For example, we performed QMD NVT simulations of formic acid at shock conditions [155], a detonation product for which there was conflicting experimental information regarding its reactivity at high shock pressures, and is a standard species considered in thermochemical code calculations. QMD NVT simulations at a state point well above the purported transition pressure for reaction showed chemical reactivity, determined from time traces of all original covalent bonds in parent formic acid, the nearest-neighbor hydrogen atom from each of the oxygen atoms in the parent molecule, as well as nearest-neighbor distances between heavy atoms in adjacent molecules. The simulations showed that hydrogens exhibited extensive mobility, migrating back and forth among species, resulting in hydrogen exchange reactions to reform formic acid or forming protonated formic acid or formate moieties. Also observed were long-lived extended networks composed of fragments and atoms from various parent molecules, which might be the early stages of polymerization under these conditions.

Other quantum-based simulation studies of materials under high temperature and pressure states also have shown similar mobility of hydrogen atoms [133–135, 162, 163], as well as charge transfer [118, 136, 164]. Similarly, we have observed "nonmolecular" hydrogen behind the shock front in overdriven shock simulations of PETN using large-scale, DFT, Born–Oppenheimer MD simulations. For example, we followed a hydrogen atom propelled forward toward the shock front, weaving through free space among a tangled mass of atoms so densely packed that chemical speciation would require a herculean effort, and would rely on a certain level of empiricism. This atom quickly migrated forward ahead of the mass flow, before it was subsequently captured by a different moiety closer to the shock front, thus arresting its free motion. In this shock simulation using QM forces, it appears to be impractical (or impossible) to define the chemistry in terms of unimolecular or bimolecular mechanisms.

While the material state in the overdriven shock simulations of PETN is at higher compression and temperature than the Wu et al. simulation of PETN at a single thermodynamic state corresponding to the experimental CJ condition [154], it is notable that a few features are similar, such as the presence of nonmolecular hydrogens. It is unfortunate that current state of the art precludes QMD simulation for sufficiently long times to simulate a steady-state detonation of an EM; thus, the material state in the reaction zone of a steady-state detonation remains to be discovered. Until novel algorithms and computational resources allowing for realistic atomistic simulations of shock initiation leading to steady-state detonation are available or advanced experimental methods are developed to interrogate the reaction zone, that question will remain unanswered. These and other studies of chemistry of materials under extreme conditions clearly support the conclusion of Wu et al. that "the traditional

approach based on molecular reactions that is commonly applied in gas-phase combustion chemistry is no longer adequate for describing chemical reactions under these extreme conditions [154]."

10.4.4 Outlook

Due to the lack of understanding of the material state and the complex chemical conversion occurring behind the shock front of a reacting EM, we argue that the most immediate need at present is to perform an extensive series of quantum-based (either DFT or DFTB) MD simulations of an EM subjected to shocks of different strengths to monitor emergent material response, specifically identifying features behind the shock front in which molecularity is retained or lost, and where chemical speciation can or cannot be determined. A lofty goal would be to compare the heterogeneous material state within a simulated detonation reaction zone against that proposed in the Nonequilibrium Zeldovich–von Neumann–Doring (NEZND) model of detonation for condensed phase explosives [165]. Pursuit of this goal is facilitated by the emergence of exascale computing [166–168], novel computational methods that will allow for QM simulations with larger system sizes and longer times (e.g., [169]), and data mining approaches [170–174] to cull crucial information directly from these atomistic simulations leading to the much-needed understanding.

Clearly, both the time and financial commitment and resources required to achieve an understanding of condensed phase chemistry is daunting. Moreover, the path forward is speculative, where we have described a possible approach for determining only the reaction mechanisms. Even more daunting is the task of determining the reaction kinetics associated with the reaction pathways. Still further, there are considerations for transitioning this information into generating a reaction model that is of practical use in the DPD-RX framework. For example, a complete reaction mechanism is required that encapsulates the reactive behavior from the initial unreacted EM through to the final product gas species. Thus, research is needed to formulate ROM for use in the DPD-RX framework that captures the important features of the detailed chemical kinetics mechanisms obtained from the atomistic simulations. Still other open-ended questions remain. If radicals, polyradicals [175], or transient states are part of the reaction mechanism, can the required input for the CG-EOS for each species be readily determined (i.e., a reference state heat of formation and temperature-dependent constant-pressure heat capacity)? Will these transient states be so short-lived that they won't play a role within the time scale of the DPD-RX time step (~5–20 fs)? If they are sufficiently long-lived, can CG models be readily developed for these species? If we develop a highly-detailed reaction mechanism, will these details be significant on the time scale of the DPD-RX simulation?

These questions provide ample opportunities for research investigations designed to afford a multiscale description of condensed phase chemical reactivity of EM at extreme conditions. Our expectation is that the ROMs will be progressively enhanced as the condensed phase reaction modeling efforts evolve. These reaction model devel-

opments will be complemented by any necessary coinciding adaptions of DPD-RX. This complementary approach provides a convenient and natural framework to incorporate the complexities arising from the coupling of microstructure with a quantum mechanical understanding of chemistry.

10.5 Hierarchical Multiscale Simulation: Reaching the Experimental Scale

Prediction of the macroscale response of energetic material, including all aspects of chemical reactivity, provides a significant motivation for continued research in multiscale modeling. Continuum "burn" (chemistry) models may often reproduce shock-to-detonation transitions when parameterized using sufficient experimental data, or when using chemical equilibrium approaches for ideal explosives, but subdetonative reactivity and deflagration-to-detonation remain difficult to predict for many systems. As chemical reactivity may be influenced by many factors, such as material EOS or microstructure, our research plan involves systematically increasing the complexity of our multiscale simulations. In this section, we will discuss: (a) common multiscale approaches, (b) properties of constitutive models for energetic materials that are currently addressed by multiscale simulation, (c) our current hierarchical multiscale approach and implementation, (d) a demonstration of our concurrent hierarchical approach, and (e) future research opportunities.

10.5.1 Multiscale Approaches

Information from particle-based simulations, such as those using the DPD-RX method, can be utilized in continuum simulations through a variety of modern multiscale approaches. We will briefly survey common multiscale approaches, generally following the taxonomy described by Tadmor and Miller [20]. In describing multiscale approaches, we will typically be describing a continuum, or macroscale, simulation that leverages information from high-fidelity, smaller length-scale calculations. In the literature, these may also be referred to as upper and lower scales, or alternatively as coarse and fine scales. We will avoid referring to the fine scale as the "microscale" in order to avoid confusion of the term with micron length scales or microsecond timescales, which nevertheless may be present in particular multiscale approaches.

10.5.1.1 Sequential Upscaling

Fast-running constitutive material models for continuum simulations may be directly parameterized from the results of fine scale simulations, much like how CG models may be constructed from the results of atomistic simulations. Examples of this include construction of an EOS for a pure material from rigorous first principles calculations [176], calculation of elastic constants for use in a continuum model [177], or the fitting of a chemistry model to a numerical description of molecular simulation results [175]. We will not discuss the sequential approach in detail; it is historically the most common approach for transferring information between scales. When carefully applied by a subject matter expert, it may provide good results for the selected problem. It is often the case that a particular upscaled material property is understood to only be applicable within a constrained range of states, i.e., the transferability problem (particularly important in force field development [178]).

10.5.1.2 Concurrent

Concurrent approaches involve performing simulations with both macroscale and fine scale methods at run time [20]. This allows for a higher fidelity description of phenomena of interest than sequential upscaling, but with increased computational expense. Fracture, for example, is difficult to realistically model at the continuum scale, but one approach is the embedding of an atomistic domain in a continuum simulation [179]. A particular property's response may be dependent upon a large number of variables, making generation of an upscaled model in advance prohibitive due to the "curse of dimensionality [14, 180]." Microstructural effects that give rise to emergent behavior may be difficult to "build in" to a predictive constitutive model [11]. In each of those cases, a concurrent multiscale approach able to directly query the results of a high-fidelity model may provide an accurate solution. Note, the nomenclature for describing concurrent simulation is highly inconsistent across the open literature. We follow Tadmor and Miller's [20] usage and further categorize concurrent multiscale simulation as "partitioned-domain" or "hierarchical".

Partitioned-Domain

Partitioned-domain approaches involve a decomposition of the simulation into multiple spatial domains, which may be overlapping. An inexpensive, less computationally costly model is used in the larger domain(s), and an expensive, more computationally costly model is used in the smaller region of critical interest [181]. Examples of this include a QM/MM simulation for modeling the active site of proteins [182], or an embedded atomistic domain in a continuum finite element mesh. Challenges for partitioned-domain approaches involve describing the "handshaking" region between different methods/models, and the accessible simulation timescales being limited by the computationally most expensive per-time-step domain (typically

also the domain requiring the smallest time step). While quite successful in solving some problems, partitioned-domain approaches may not be applicable to problems where the domain requiring high-fidelity information is itself macroscale in size; the high-fidelity, expensive model could consume nearly the entire extent of the system being simulated. Another limitation is when long timescales need to be accessed. For example, some partitioned-domain methods are limited by the timescale of the step size in the expensive simulation (e.g., continuum cycles operating at MD time steps, roughly ~1 fs), although recent research has attempted to address this issue [179].

Hierarchical

Hierarchical approaches often involve the interleaving of macroscale and fine scale simulations [13, 183–185]. A macroscale simulation, such as a continuum finite element simulation, may require information about its elements from the fine scale at each time step [186]. This information may be provided from constrained fine scale simulations run in-between continuum time steps. This information exchange between scales characterizes a hierarchical approach. An example of this from the field of computational mechanics is the FE^2 simulation, where two finite element simulations are performed, with the fine scale being a much more highly resolved "representative volume element" (RVE) [187]. Intensive properties of the RVE may be used at the macroscale in a technique called computational homogenization [188]. More general mathematical frameworks for hierarchical simulation include the "equation-free" approach and heterogeneous multiscale method (HMM) [184, 189, 190]. In HMM calculations, generalized macroscale governing equations that rely upon a set of variables may have missing variables provided by constrained fine scale calculations. The constraints and simulations necessary at the fine scale are application-specific, and left for the subject matter expert to determine [189]. Using an HMM approach, one may calculate many different material properties across the entire macroscale domain using high-fidelity fine scale simulations. An example we will describe later in this section is calculating EOS response from particle-based simulations.

10.5.2 Constitutive Material Models

We briefly describe two common components of a constitutive model for energetic materials, which may be described by a multiscale model. Other possible components of a material model may include (but are not limited to) models for failure, elasticity, plasticity, yield strength, hardening, as well as properties such as thermal conductivity, melt curves, heat capacity, or viscosity. In a shock-to-detonation transition, brittle failure or thermal conductivity may not be a concern for modeling; the material will detonate on a short timescale and those properties may not affect

the transition. However, every continuum simulation for energetic material response requires an EOS, even if the material does not undergo reaction. Therefore we start with a discussion of the material EOS, and then discuss chemistry, since energetic materials will eventually leverage their energy-releasing chemistry during physically relevant simulations.

10.5.2.1 Equation of State

First and foremost for our application is the material EOS. This is the relationship between material energy, density, temperature, and pressure. A simple example is the ideal gas law for a gaseous EOS. Pressure is often calculated through an analytical EOS such as the Mie-Grüneisen equation, Jones–Wilkins–Lee EOS, or a number of other forms [191]. More complicated recent examples include the use of the Peng–Robinson EOS for multiphase mixtures [192], or construction of a free energy-based EOS for solid RDX [176]. In many material models, the temperature may not actually be calculated and is not present in the continuum governing equations. The temperature may be calculated if a cold curve, or the static lattice energy as a function of volume, is available. Tabulated forms such as Livermore EOS tables or SESAME tables are also used in modern hydrocodes, which may include data for all relevant state variables (including temperature). An accurate EOS is critical for calculation of peak shock pressure and related state variables in a continuum simulation, or for stress–strain response at a variety of strain rates. Calculation of realistic stress–strain curves requires both accurate elasticity and plasticity models before the onset of failure. Calculation of the EOS is particularly challenging for energetic materials, as chemical composition will change over the course of a reactive event, such as a detonation. An ideal steady-state detonation described by Chapman–Jouguet theory is at the state point where the Rayleigh line of the unreacted products is tangent to the shock Hugoniot for the product gas [193]. Calculation of those states, and therefore the detonation properties of an energetic material, requires an accurate EOS for unreacted material and any species in the reaction mechanism leading to the final products.

10.5.2.2 Chemistry

While continuum simulations of metals, ceramics, or some composites (e.g., fiber composites at low strain rate) may not need to consider chemical reactivity, energetic materials release stored energy through chemical reactions. When modeling explosives, phenomenological models such as the Tarver "ignition and growth" reactive flow model [165, 194] are often used to describe detonation kinetics. In that model, progress from reactants to products depends upon material density, pressure, and amount previously reacted. The reactants and products are described by separate EOS models. Complex hydrocodes also have support for advanced chemistry models that may explicitly account for many chemical compounds and complicated chemi-

cal kinetics, including chemical equilibrium detonation models [195]. In the absence of robust experimental data, it may be difficult to parameterize any type of chemistry model, motivating the need for multiscale modeling. Further, phenomenological models such as the ignition and growth model are less useful for some problem domains; for example, a model that describes shock-to-detonation may not provide predictive physical insight regarding the effects of low-velocity sub-detonative impacts on an energetic material. Therefore, phenomenological models are developed to model particular classes of problems. Significant progress has been made in developing models for thermal cook-off [8, 196] or reactions due to low-speed impact [197]. In principle, a high-fidelity multiscale model can be used to describe the response to loading at a variety of conditions, including the key chemical processes in a material [171, 198]. Advances in the DPD-RX methodology (Sect. 10.3) provide a path forward for high-fidelity modeling at micron length scales that may address conditions ranging from nonreactive, low-speed impact to shock-to-detonation transitions.

10.5.3 Hierarchical Multiscale Simulation

10.5.3.1 Definition of Scales

In this section, we will describe our particular approach for bridging to continuum, which we refer to as "hierarchical multiscale simulation" (HMS). The macroscale in our work is a continuum, Lagrangian finite element simulation in ALE3D [171, 199]. The fine scale in our work generates results from the set of DPD variants implemented in LAMMPS and the CG-RDX model described above. The constitutive material model in ALE3D receives its EOS information from these fine scale simulations. We will also describe results where chemistry is provided from fine scale simulations. This combination of macroscale and fine scale defines a concurrent, hierarchical approach using the Heterogeneous Multiscale Method. A software framework, referred to as the HMS framework, handles communication and transformation of information between the macroscale and fine scale [200, 201]. The HMS framework also handles computational aspects of the multiscale implementation, such as queuing of the fine scale calculations and storage of the fine scale results. Figure 10.7 provides a conceptual representation of the connection between scales, with the HMS framework handling communication between the macroscale and fine scale, and requests being dispatched from the macroscale on a per-element basis.

10.5.3.2 Machine Learning

In some cases, direct evaluation of the fine scale for every element at every continuum time step (or "cycle") may be prohibitively expensive for simulations with millions of finite elements, over many hundreds of continuum cycles. Consider the case of a 1

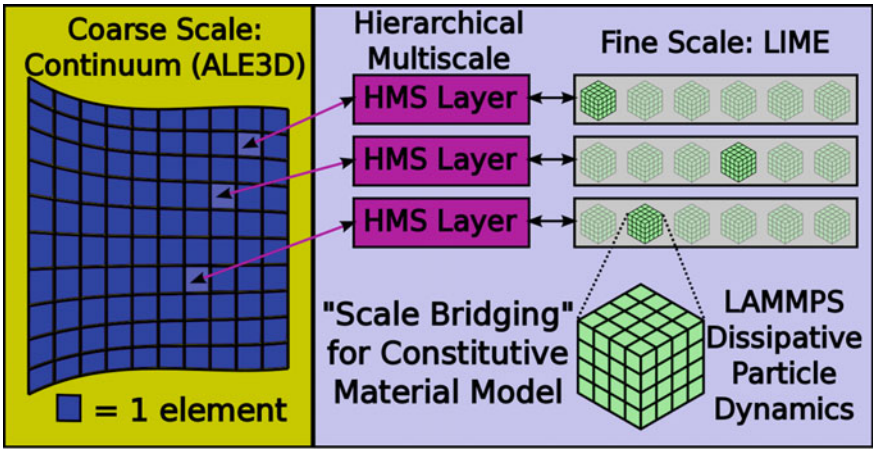

Fig. 10.7 Conceptual representation of the connection between the macroscale, the HMS framework, and the fine scale

million element simulation run for 7000 cycles, with a fine scale that requires 3 min and 64 cores for solution (for one element, at one cycle). On a 100,000 core machine, completion of that simulation would take over 25 years. In order to make our HMS approach computationally tractable, the HMS framework implements a feature to leverage previously computed fine scale results. The central idea is that a set of such previously computed fine scale results may be used to approximate the result for a new property calculation, if the new fine scale state is easily interpolated from previously computed states. Interpolation may be many orders of magnitude faster than an actual fine scale evaluation. Publications variously describe this general approach as surrogate modeling, adaptive sampling, or machine learning [180, 200, 202–209]. When used with a database managed by the HMS framework that is expanding over time (i.e., over the course of the macroscale simulation), where additional information in the database improves interpolation efficiency and accuracy, we consider this to be regression via supervised machine learning. HMS applications requiring millions of elements and hundreds of cycles become computationally tractable with an efficient machine learning implementation. It is critical that the development of this data-driven model is done in close coordination with a subject matter expert for the underlying physics-driven model, otherwise unphysical results may go unnoticed. In short, theory and data should work hand in hand [172].

10.5.3.3 Speculative Evaluations

The use of machine learning to make problems tractable introduces a new challenge for HPC environments, where the number of cores available is not a severe constraint. As the efficiency of the machine learning algorithm (i.e., its interpolation rate) may

vary from cycle to cycle, the number of required fine scale evaluations will fluctuate. If the number of cores requested for the job exceeds the number of cores necessary for fine scale evaluations, then some remaining cores may be idle. This inefficiency may be overcome through the launching of "speculative" evaluations of the fine scale model on those otherwise idle cores. While not directly used in constitutive model evaluations for the current cycle, these speculative evaluations may be added to the HMS framework database of fine scale results. Additional data in that database will improve the efficiency and accuracy of future machine-learned model evaluations, therefore potentially decreasing wall clock run time and increasing the overall fidelity of the simulation. This is particularly important, as wall clock run time may be determined by the slowest element; improvement of the fine scale database to a point where no fine scale evaluations are needed for a particular cycle results in impressive wall clock speedups. Speculative HMS may also leverage batch schedulers that allow changes in the number of cores available for jobs that are currently running; additional speculative evaluations could be initiated if there are idle nodes on a supercomputer, or the number of speculative evaluations was lowered for the case in which a higher priority job is needed to acquire additional batch nodes. The inherently parallel nature of fine scale evaluations—each fine scale simulation is independent of others—makes speculative HMS easily amenable to full utilization of petascale and potentially even exascale HPC resources, given a sufficiently complicated problem and expensive fine scale evaluations.

10.5.3.4 The HMS Framework

Key to the effective execution of this HMS strategy is the software framework that interfaces the macroscale and fine scale [200, 201]. Typically, simulation software is not written with concurrent, hierarchical multiscale coupling in mind. The software is most often run in a standalone manner using well-documented material models, such as analytical forms available in hydrocodes or empirical potential forms built-in to MD programs. Therefore, communicating constraints and results between those programs is a software engineering task. This framework is also responsible for the machine learning (or surrogate model) and scheduling of fine scale evaluations, which are computational science problems. While not adding significant computational overhead, the HMS framework is responsible for handling the parallel execution of the updates to the fine scale database (evaluations necessary for the macroscale model), as well as the updates to the machine-learned model. It should be sufficiently general that if the HMS requirements change, e.g., additional macroscale variables are requested for evaluation in a more complicated fine scale model, then large parts of the software framework do not need to be rewritten. Similarly, it should be flexible enough to allow for easy changes to the machine learning method or its hyperparameters and to accommodate restarts to simulations that are terminated due to hardware error or queue run time limitations. In general, the design and implementation of the HMS framework is an effort that is distinct from, but as important as, the design and implementation of the fine scale model.

10.5.4 HMS with LIME as the Fine Scale

In this final section, we describe HMS results using a fine scale model for RDX. The fine scale solver we use is the LAMMPS Integrated Materials Engine (LIME) [210], an automation and analysis tool written in Python, and developed specifically for our HMS effort. LIME instantiates, executes, and returns results from DPD simulations using our CG model for RDX. In an HMM review article, E. and co-workers describe the design of the fine scale solver as "often the most difficult step, and is subject to continuous improvement [189]." Fine scale solvers must reliably return an accurate result to the HMS framework without human intervention in a minimal amount of time, over any range of inputs that may be encountered during the macroscale simulation. Further, execution of many fine scale solvers must effectively scale—task parallelism leads to efficient leveraging of supercomputing resources [186]. If the fine scale solver is extremely costly for reading or writing many files or large files to a shared file system, i.e., input and output (I/O) intensive, then simultaneous execution of thousands of fine scale solvers may degrade HMS performance. This may also occur for MPI initialization of programs [211]. Further, jobs unrelated to the multiscale simulation may also be degraded. As such careful design of the fine scale solver is necessary.

10.5.4.1 Nonreactive Case

The nonreactive case of HMS using LIME utilizes a CG model for RDX and DPD-E. In this simulation, the macroscale requires EOS information from the fine scale. In particular, it needs temperature and pressure (T, P) as a function of energy and density (E, ρ). The pressure desired is the hydrostatic component of the stress tensor. The hydrostatic nature of the response and the two input state variables provide sufficient constraints to allow for the construction of the fine scale problem. The temperature and pressure returned may be considered to be equilibrium values. This allows for decoupling of the macroscale and fine scale in both length (the fine scale simulation will have a smaller volume than the macroscale element) and time (equilibrium simulations at the fine scale may have a smaller simulation time than the duration of macroscale time steps). The fine scale solver must instantiate a DPD simulation with the same energy and density as the macroscale inputs. It must then equilibrate the simulation cell. Although equilibration may be assumed for sufficiently long equilibration periods, properly detecting equilibration is nontrivial and extremely useful for performing fine scale simulations in minimal amounts of wall clock time. After the cell is equilibrated, the solver must collect enough data to produce accurate ensemble averages for temperature and pressure, and return those averages to the HMS framework. Additional data, such as the standard error and variance of the ensemble averages, may also be returned. Those values may be used for uncertainty quantification at the macroscale. When information from microscale/mesoscale simulations is used to determine material response in continuum simulations, the ideal

continuum model would reproduce the exact result of the fine scale model, if the two models/methods were used to simulate the same physical system over the same amount of time. In general, correspondence of observable properties between scales is a key component of validating a multiscale model.

In Fig. 10.8, we demonstrate this correspondence of results for the *P*-*V* and *T*-*V* planes of the Hugoniot with our CG-RDX model. The sets compared are data provided by LIME and used in an ALE3D plate impact simulation, and data from longer duration results purely from DPD-E simulation in LAMMPS. The T-V plane is particularly sensitive to error. For example, if the simulation cell does not have approximately equal pressure in each cardinal direction when generating data to be used in ALE3D, then the LAMMPS and ALE3D results will diverge by several Kelvin. LIME carefully monitors the normal directions of the pressure tensor in order to ensure they are roughly equal, therefore that error is not present in Fig. 10.8. Additionally, a very small difference is observed when a yield stress (strength model) is present in the ALE3D simulation. Disabling this restores near exact agreement between the sets.

Because temperature determines chemistry in our fine scale model and is the more sensitive property for bridging scales, it is prudent to investigate the accuracy of temperature calculations in further detail. Figure 10.9 demonstrates the standard error of the mean, or the sampling accuracy, of temperature for our fine scale model using LIME. The axes in Fig. 10.9 reflect the inputs to LIME: finite element energy

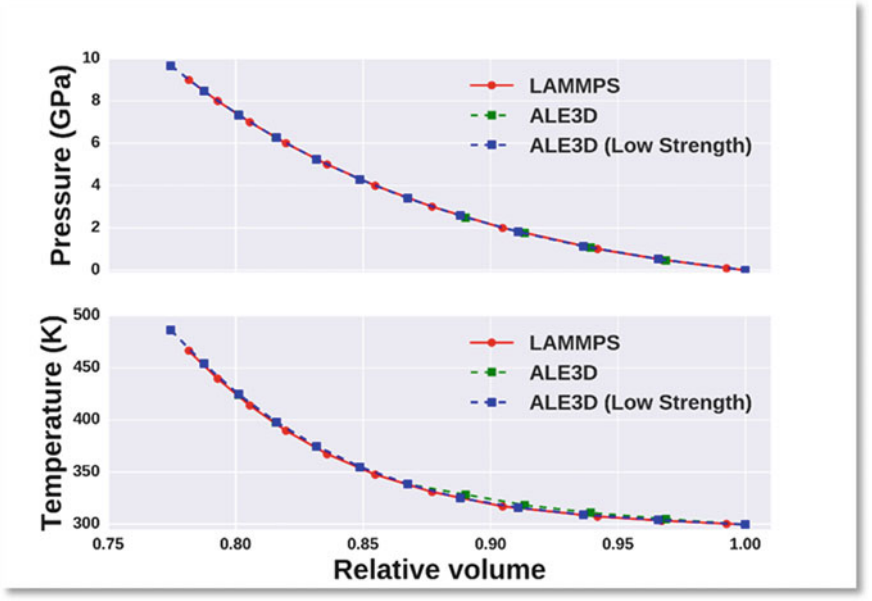

Fig. 10.8 *P*-*V* and *T*-*V* planes of the Hugoniot for particle-based simulations (LAMMPS) and continuum simulations (ALE3D) driven by LIME EOS tables

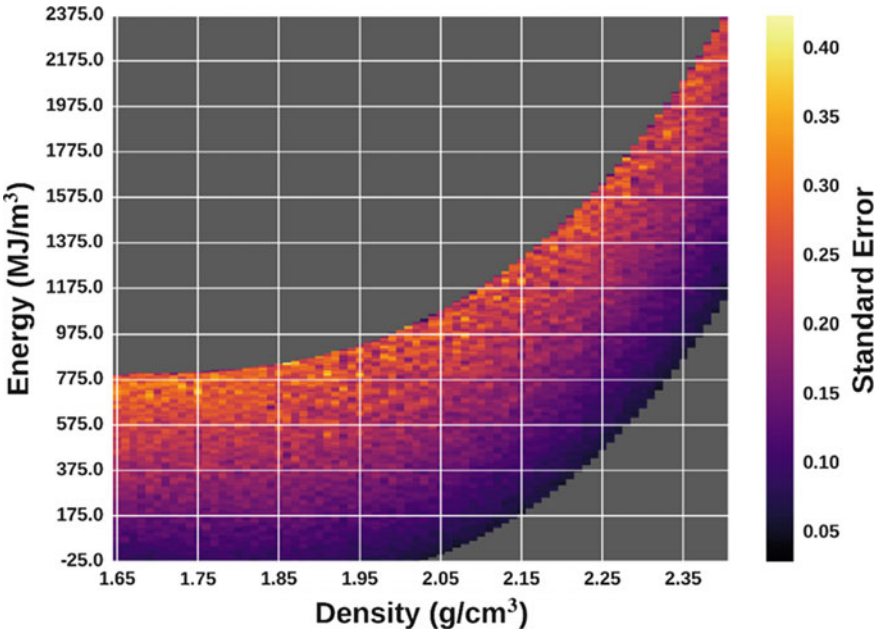

Fig. 10.9 Standard error of the mean for temperature over a range of LIME EOS calculations

and density. In general, LIME provides results with 0.5 K or better accuracy in temperature for a given state point. As would be expected, systems that are higher in energy (hotter) have larger error, since we are demonstrating absolute error and not relative error.

Understanding the efficiency of fine scale simulations across a wide variety of state points is important, in that it determines both a limiting factor for wall clock time of the macroscale simulation, and may reveal a challenge for automation of fine scale calculations. In Fig. 10.10 we examine the total number of DPD-E time steps (equilibration and production, combined) performed during state point evaluations across the wide-ranging surface of energy and density. While the vast majority of state point evaluations using LIME require fewer than ~9000 total DPD-E time steps, there is a significant cluster in the 1.85–2.15 g/cm^3 range at energies corresponding to temperatures of over 500 K, where many more time steps are needed in order to converge LIME. If it would be common for simulations to explore that part of state space, then the algorithms and heuristics in LIME could be further tuned in order to accelerate convergence for those state points.

Putting it all together for the nonreactive case, we demonstrate a Lagrangian finite element Taylor anvil impact simulation using ALE3D as the macroscale and LIME as the fine scale for the material EOS. In Figs. 10.11 and 10.12, snapshots from 2D axisymmetric impact simulations are shown with elements colored by pressure, demonstrating pressure waves traveling through the material and deformation at

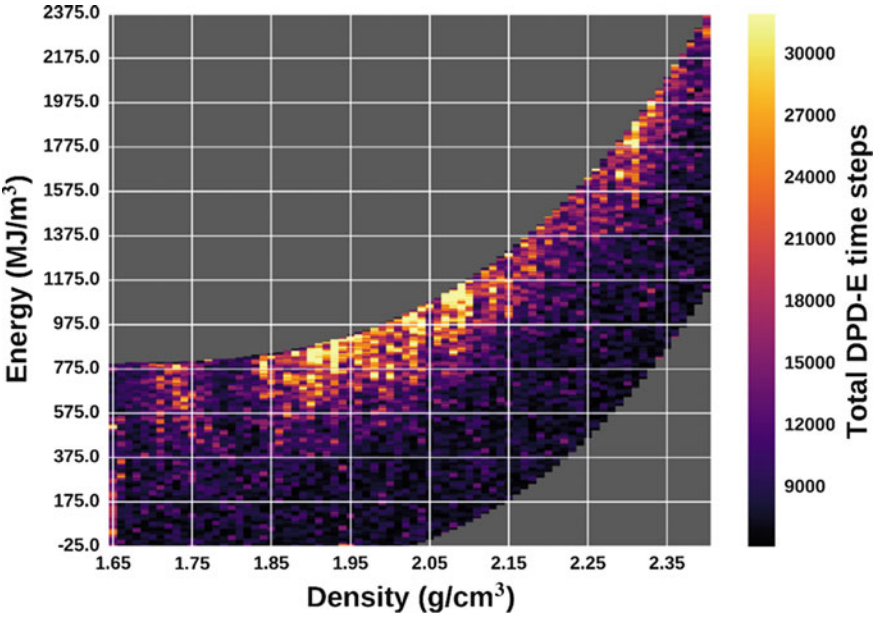

Fig. 10.10 Total number of DPD-E time steps necessary for LIME convergence over a range of state point calculations

material edges that are impacting the hard wall. The simulation in Fig. 10.11 used LIME for EOS calculations in each of the 1600 elements. These calculations were performed "on the fly", meaning that LIME was called during the HMS simulation, for each element, at each cycle. The simulation in Fig. 10.12 also used LIME as the fine scale, but used a machine learning method for statistical regression in the HMS framework in order to provide estimates of LIME response within a controllable error tolerance. The regression method of choice for our HMS framework is kriging, also known as Gaussian process regression, and was previously demonstrated in a study examining a two-scale model for crystal plasticity [200]. This allowed the simulation in Fig. 10.12 to use one million elements for its mesh (a 625× increase in mesh size), without needing to explicitly call LIME for each of those elements at every cycle. Comparing the figures, for this case, it is evident that higher mesh resolutions are critical for resolving physical phenomena in continuum simulations, where the separation of elastic and plastic waves is visible in Fig. 10.12, while not visible in Fig. 10.11.

10.5.4.2 Reactive Case

The second example of HMS using LIME is that of a plate impact test using the CG-RDX model and DPD with reactions (DPD-RX) method described above in

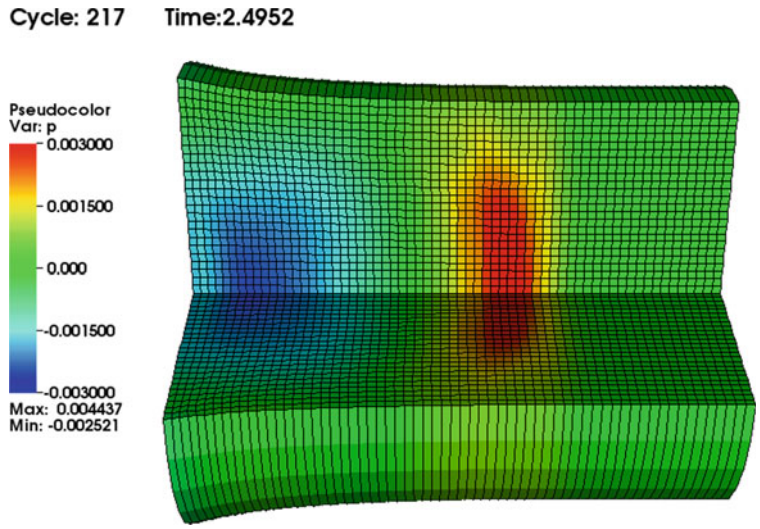

Fig. 10.11 Taylor impact test simulation, colored by pressure, with 1600 elements. EOS response for each element was calculated with LIME "on the fly" every cycle. Time units are microseconds and pressure units are megabar

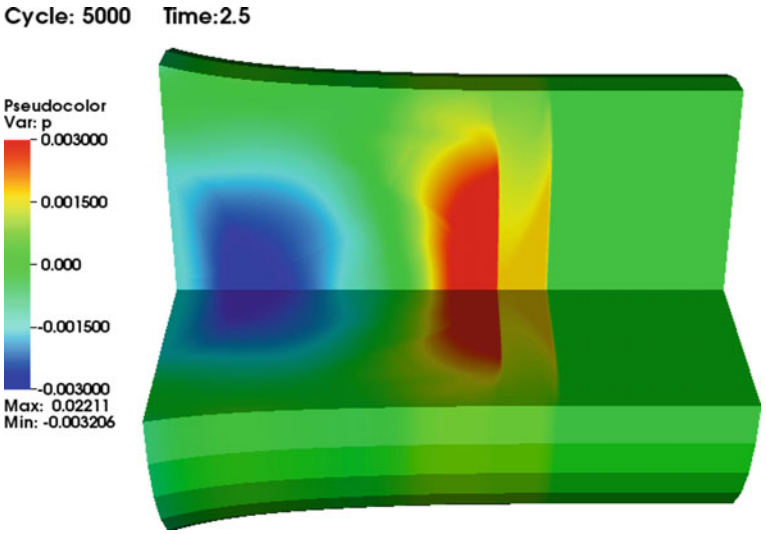

Fig. 10.12 Taylor impact test simulation, colored by pressure, with one million elements. EOS response for each element was calculated using a combination of LIME "on the fly" and machine-learned responses. Time units are microseconds and pressure units are megabar

Sects. 10.2 and 10.3, respectively. In this simulation, the macroscale requires not only EOS information from the fine scale, but also chemical species information, an additional nine variables given our reaction model described in Sect. 10.3. However, the time evolution of chemical kinetics under shock infers that the fine scale may no longer be assumed to be in an equilibrium state. Therefore, a similar instantiation and equilibration scheme may be followed in LIME (adjusted for input chemical species from the macroscale), but production data is collected in "lock step" with the macroscale; in particular, the fine scale solver covers the same production simulation time as the macroscale time step. HMS plate impact simulations, such as the snapshot in Fig. 10.13, demonstrate the consumption of RDX and temperature rises similar in magnitude to those observed in DPD-RX simulation, but systematically lower. This is believed to be in part due to the effects of computational homogenization when a wave has only partially passed through a many-micron wide finite element. Resolving differences between reactions at the macroscale and fine scale and solving the "scale-bridging in time" problem for the nonequilibrium case are active areas of research for us.

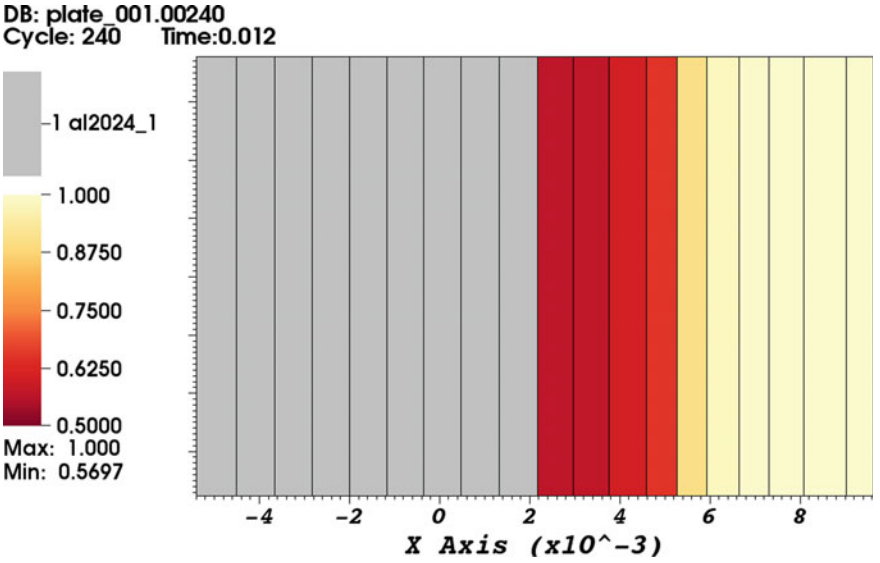

Fig. 10.13 Plate impact simulation, colored by amount of RDX consumed (red scheme, 1.0 = pure RDX, 0.0 = all RDX consumed) and material type (gray, aluminum). This demonstrates direct use of chemistry from fine scale simulations during a continuum shock impact simulation. Only elements near where chemistry is occurring are displayed. Time units are microseconds and length units are centimeters

10.5.5 Outlook

Going forward, many challenges need to be overcome for our HMS approach applied to energetic materials. Simulations to date have relied on an idealized description of RDX as a homogenous, defect-free single-crystal material. However, as described at the beginning of this chapter, it is known that for real energetic materials, initiation thresholds are determined by a number of factors such as polycrystalline grain size, shear, porosity, amount and types of binder or plasticizer present, or more broadly, any inhomogeneities present [1, 2, 6, 117, 194, 212–220]. Incorporating those effects into an HMS model will require continued research and development of the fine scale particle-based models, and then leveraging of those models in an HMS scheme that utilizes additional history variables to describe each of those components of the material microstructure. Capturing all of those effects in a single microscale RVE may be difficult or impossible, requiring use of several statistical volume elements to capture a variety of effects and then return weighted results to the macroscale [221–224]. Including over a dozen history variables for descriptions of microstructure and chemistry in an automated fine scale calculation also leads to new challenges for machine learning in a high-dimensional space, the so-called "curse of dimensionality [14, 180, 225–229]." Regardless of the multiscale approach chosen, currently there is no immediately apparent approach to model the complex reactive response of energetic materials across all possible insults. However, with further developments, HMS provides a viable and promising path forward for accurate, high fidelity simulations in the future.

10.6 Concluding Remarks

Advances in multiscale modeling and simulation methodologies are beginning to make possible virtual design and performance assessment of EM, before actual production, enabling modeling and analysis of complex phenomena across multiple time and length scales. We have described our own developmental efforts to predict the dynamic behavior of EM at all relevant length scales that will lead to understanding of the various dynamic processes, properties, and mechanisms for energetic material response under the full range of conditions. Microstructure plays a dominant role in the macroscale response of the EM, however, computational capabilities have been lacking at the microscale. We described our efforts to fill this computational capability gap through the development of CG models and methods that can simulate microstructure evolution (including effects of chemistry) in response to various stimuli. Upon upscaling of these microscale tools into the macroscale models, the effects that microstructural heterogeneities impose on macroscopic events can be captured. We described multiscale modeling methodologies capable of coupling behaviors from the fine scale to the macroscale, including our choice of a concurrent,

hierarchical multiscale approach, and the computational simulation framework into which simulations at the various scales are effectively integrated.

Relative to atomistic and continuum approaches used to simulate EMs, our microscale and hierarchical multiscale efforts are in the nascent stage of development. Currently, we have demonstrated proof of concept calculations and provided paths forward for advancing the methodologies. We are proceeding in a straightforward methodical manner, and while much more work is needed, our efforts continue to evolve, where progress continues to be promising. Although the effects of the loss of fidelity due to coarse-graining have yet to be rigorously quantified for our models, estimates of the computational gains are encouraging. If we consider MD using the ReaxFF force field as the most viable model comparison for the detailed simulation of microstructure evolution with chemistry, estimates of the computational costs savings of our microscale approaches are on the order of 10^4 in speedup. Such gains allow us to move beyond the simulation of isolated ideal microstructure and begin simulating microstructure typically found in actual EM composites.

We described deficiencies of various components of our efforts, with an emphasis on the reaction models. We believe that future work should focus on the development of reduced-order models that properly depict chemistry of condensed phase materials under extreme temperatures and pressures. Key development needed for our CG models is a more accurate modeling of the plastic response and improvement in the transferability of the product gas mixture model. A next stage development for our CG methods will focus on a more complete representation of species mass diffusion. For the multiscale hierarchical tools, further work is needed on novel statistical sampling of microstructural features at the fine scale, and obtaining an understanding of error propagation and uncertainty quantification across the scales. This includes uncertainties on dynamic yield behavior, fracture behavior, mechanical/chemical physics at extreme states, plastic deformation, anisotropic crystal properties, material slip, and contact behavior—all of which affect the behavior of an EM.

We hope that the description of the research challenges will inspire further development of innovative models and methods, leading to a robust predictive multiscale modeling and simulation capability that will describe EM response under the full range of conditions. Our tools are built around a general computational framework, so that they can be extended to other material systems with moderate modification. Therefore, while we hope our efforts will advance EM design, we also hope that they will be used to study materials beyond EM.

References

1. Baer MR (2002) Modeling heterogeneous energetic materials at the mesoscale. Thermochim Acta 384:351–367
2. Baer MR (2007) Mesoscale modeling of shocks in heterogeneous reactive materials. In: Horie Y (ed) Shock wave science and technology reference library, vol 2. Springer, pp 321–356

3. Barton NR, Winter NW, Reaugh JE (2009) Defect evolution and pore collapse in crystalline energetic materials. Model Simul Mater Sci Eng 17(3):035003. https://doi.org/10.1088/0965-0393/17/3/035003
4. Jackson TL, Hooks DE, Buckmaster J (2011) Modeling the microstructure of energetic materials with realistic constituent morphology. Propel Explos Pyrotech 36(3):252–258. https://doi.org/10.1002/prep.201000096
5. Akiki M, Menon S (2015) A model for hot spot formation in shocked energetic materials. Combust Flame 162(5):1759–1771. https://doi.org/10.1016/j.combustflame.2014.11.037
6. Austin RA, Barton NR, Reaugh JE, Fried LE (2015) Direct numerical simulation of shear localization and decomposition reactions in shock-loaded HMX crystal. J Appl Phys 117(18):185902. https://doi.org/10.1063/1.4918538
7. Rai NK, Udaykumar HS (2015) Mesoscale simulation of reactive pressed energetic materials under shock loading. J Appl Phys 118(24):245905. https://doi.org/10.1063/1.4938581
8. Nichols AL, Becker R, Howard WM, Wemhoff A, Elert M, Furnish MD, Anderson WW, Proud WG, Butler WT (2009) Toward improved fidelity of thermal explosion simulations, AIP Conf Proc 1195:229. https://doi.org/10.1063/1.3295110
9. Geers MGD, Kouznetsova VG, Brekelmans WAM (2010) Multi-scale computational homogenization: trends and challenges. J Comput Appl Math 234(7):2175–2182. https://doi.org/10.1016/j.cam.2009.08.077
10. Ghosh S (2015) Foundational aspects of a multi-scale modeling framework for composite materials. Integrating Mater Manuf Innov 4(1). https://doi.org/10.1186/s40192-015-0036-x
11. Geers MGD, Yvonnet J (2016) Multiscale modeling of microstructure–property relations. MRS Bull 41(08):610–616. https://doi.org/10.1557/mrs.2016.165
12. Yip S, Short MP (2013) Multiscale materials modelling at the mesoscale. Nat Mater 12(9):774–777. https://doi.org/10.1038/nmat3746
13. Elliott JA (2013) Novel approaches to multiscale modelling in materials science. Int Mater Rev 56(4):207–225. https://doi.org/10.1179/1743280410y.0000000002
14. Unger JF, Eckardt S (2011) Multiscale modeling of concrete. Arch Comput Methods Eng 18(3):341–393. https://doi.org/10.1007/s11831-011-9063-8
15. McDowell DL (2010) A perspective on trends in multiscale plasticity. Int J Plast 26(9):1280–1309. https://doi.org/10.1016/j.ijplas.2010.02.008
16. Kouznetsova V, Brekelmans WAM, Baaijens PT (2001) An approach to micro-macro modeling of heterogeneous materials. Comput Mech 27:37–48
17. Tappan A (2013) There's plenty of room in the middle—microenergetics, the mesoscale, and interfaces. Propel Explos Pyrotech 38:475
18. Frenkel D, Smit B (2002) Understanding molecular simulation, 2nd edn. Academic Press, San Diego, CA
19. Belytschko T, Liu WK, Moran B, Elkhodary KI (2014) Nonlinear finite elements for continua and structures. Wiley Ltd., The Atrium, Southern Gate, Chichester, West Sussex, PO19 8SQ, United Kingdom
20. Tadmor EB, Miller RE (2011) Modeling materials: continuum, atomistics, and multiscale techniques. Cambridge University Press, University Press, Cambridge
21. Farah K, Muller-Plathe F, Bohm MC (2012) Classical reactive molecular dynamics implementations: state of the art. ChemPhysChem 13(5):1127–1151. https://doi.org/10.1002/cphc.201100681
22. Chenoweth K, van Duin AC, Goddard III WA (2008) ReaxFF reactive force field for molecular dynamics simulations of hydrocarbon oxidation. J Phys Chem A 112:1040–1053
23. van Duin AC, Dasgupta S, Lorant F, Goddard WA (2001) ReaxFF: a reactive force field for hydrocarbons. J Phys Chem A 105:9396–9409
24. Shan T-R, Wixom RR, Thompson AP (2016) Extended asymmetric hot region formation due to shockwave interactions following void collapse in shocked high explosive. Phys Rev B 94(5):054308. https://doi.org/10.1103/physrevb.94.054308
25. Monaghan JJ (1992) Smoothed particle hydrodynamics. Annual Rev Astronomy Astrophys 30:543–574

26. Müller-Plathe F (2002) Coarse-graining in polymer simulation: from the atomistic to the mesoscopic scale and back. ChemPhysChem 3:754–769
27. Tozzini V (2005) Coarse-grained models for proteins. Curr Opin Struct Biol 15(2):144–150
28. Peter C, Kremer K (2009) Multiscale simulation of soft matter systems—from the atomistic to the coarse-grained level and back. Soft Matter 5(22):4357. https://doi.org/10.1039/b912027k
29. Noid WG (2013) Perspective: coarse-grained models for biomolecular systems. J Chem Phys 139(9):090901. https://doi.org/10.1063/1.4818908
30. Reith D, Putz M, Müller-Plathe F (2003) Deriving effective mesoscale potentials from atomistic simulations. J Comput Chem 24:1624–1636
31. Pagonabarraga I, Hagen MHJ, Frenkel D (1998) Self-consistent dissipative particle dynamics algorithm. Europhys Lett 42:377–382
32. Pagonabarraga I, Frenkel D (2001) Dissipative particle dynamics for interacting systems. J Chem Phys 115(11):5015. https://doi.org/10.1063/1.1396848
33. Trofimov SY, Nies ELF, Michels MAJ (2002) Thermodynamic consistency in dissipative particle dynamics simulations of strongly nonideal liquids and liquid mixtures. J Chem Phys 117(20):9383. https://doi.org/10.1063/1.1515774
34. Schommers W (1973) A pair potential for liquid rubidium from the pair correlation function. Phys Lett A 43(2):157
35. Izvekov S, Voth GA (2005) A multiscale coarse-graining method for biomolecular systems. J Phys Chem B 109:2469–2473
36. Izvekov S, Voth GA (2005) Multiscale coarse graining of liquid-state systems. J Chem Phys 123(13):134105. https://doi.org/10.1063/1.2038787
37. Noid WG, Chu JW, Ayton GS, Krishna V, Izvekov S, Voth GA, Das A, Andersen HC (2008) The multiscale coarse-graining method. I. A rigorous bridge between atomistic and coarse-grained models. J Chem Phys 128(24):244114. https://doi.org/10.1063/1.2938860
38. Noid WG, Liu P, Wang Y, Chu JW, Ayton GS, Izvekov S, Andersen HC, Voth GA (2008) The multiscale coarse-graining method. II. Numerical implementation for coarse-grained molecular models. J Chem Phys 128(24):244115. https://doi.org/10.1063/1.2938857
39. Izvekov S, Chung PW, Rice BM (2010) The multiscale coarse-graining method: assessing its accuracy and introducing density dependent coarse-grain potentials. J Chem Phys 133(6):064109. https://doi.org/10.1063/1.3464776
40. Lu L, Izvekov S, Das A, Andersen HC, Voth GA (2010) Efficient, regularized, and scalable algorithms for multiscale coarse-graining. J Chem Theory Comput 6:954–965
41. Izvekov S, Chung PW, Rice BM (2011) Particle-based multiscale coarse graining with density-dependent potentials: application to molecular crystals (hexahydro-1,3,5-trinitro-s-triazine). J Chem Phys 135(4):044112. https://doi.org/10.1063/1.3607603
42. Shell MS (2008) The relative entropy is fundamental to multiscale and inverse thermodynamic problems. J Chem Phys 129(14):144108. https://doi.org/10.1063/1.2992060
43. Das A, Andersen HC (2009) The multiscale coarse-graining method. III. A test of pairwise additivity of the coarse-grained potential and of new basis functions for the variational calculation. J Chem Phys 131(3):034102. https://doi.org/10.1063/1.3173812
44. Krishna V, Noid WG, Voth GA (2009) The multiscale coarse-graining method. IV. Transferring coarse-grained potentials between temperatures. J Chem Phys 131(2):024103. https://doi.org/10.1063/1.3167797
45. Das A, Andersen HC (2010) The multiscale coarse-graining method. V. Isothermal-isobaric ensemble. J Chem Phys 132(16):164106. https://doi.org/10.1063/1.3394862
46. Larini L, Lu L, Voth GA (2010) The multiscale coarse-graining method. VI. Implementation of three-body coarse-grained potentials. J Chem Phys 132(16):164107. https://doi.org/10.1063/1.3394863
47. Lu L, Voth GA (2011) The multiscale coarse-graining method. VII. Free energy decomposition of coarse-grained effective potentials. J Chem Phys 134(22):224107. https://doi.org/10.1063/1.3599049
48. Das A, Andersen HC (2012) The multiscale coarse-graining method. VIII. Multiresolution hierarchical basis functions and basis function selection in the construction of coarse-grained force fields. J Chem Phys 136(19):194113. https://doi.org/10.1063/1.4705384

49. Das A, Andersen HC (2012) The multiscale coarse-graining method. IX. A general method for construction of three body coarse-grained force fields. J Chem Phys 136(19):194114. https://doi.org/10.1063/1.4705417
50. Das A, Lu L, Andersen HC, Voth GA (2012) The multiscale coarse-graining method. X. Improved algorithms for constructing coarse-grained potentials for molecular systems. J Chem Phys 136(19):194115. https://doi.org/10.1063/1.4705420
51. Izvekov S (2017) Mori-Zwanzig theory for dissipative forces in coarse-grained dynamics in the Markov limit. Phys. Rev. E 95(1):013303. https://doi.org/10.1103/physreve.95.013303
52. Moore JD, Barnes BC, Izvekov S, Lísal M, Sellers MS, Taylor DE, Brennan JK (2016) A coarse-grain force field for RDX: density dependent and energy conserving. J Chem Phys 144(10):104501. https://doi.org/10.1063/1.4942520
53. Kinjo T, Hyodo SA (2007) Equation of motion for coarse-grained simulation based on microscopic description. Phys Rev E Stat Nonlin Soft Matter Phys 75(5 Pt 1):051109. https://doi.org/10.1103/physreve.75.051109
54. Darve E, Solomon J, Kia A (2009) Computing generalized Langevin equations and generalized Fokker-Planck equations. Proc Natl Acad Sci USA 106:10884–10889
55. Hijon CEP, Vanden-Eijnden E, Delgado-Buscalioni R (2010) Mori-Zwanzig formalism as a practical computational tool. Faraday Discuss 144:301–322
56. Hoogerbrugge PJ, Koelman JMVA (1992) Simulating microscopic hydrodynamic phenomena with dissipative particle dynamics. Europhys Lett (EPL) 19(3):155–160
57. Koelman JMVA, Hoogerbrugge PJ (1993) Dynamic simulations of hard-sphere suspensions under steady shear. Europhys Lett 21:363–368
58. Hijon C, Serrano M, Espanol P (2006) Markovian approximation in a coarse-grained description of atomic systems. J Chem Phys 125(20):204101. https://doi.org/10.1063/1.2390701
59. Trement S, Schnell B, Petitjean L, Couty M, Rousseau B (2014) Conservative and dissipative force field for simulation of coarse-grained alkane molecules: a bottom-up approach. J Chem Phys 140(13):134113. https://doi.org/10.1063/1.4870394
60. Izvekov S, Rice BM (2014) Multi-scale coarse-graining of non-conservative interactions in molecular liquids. J Chem Phys 140(10):104104. https://doi.org/10.1063/1.4866142
61. Louis AA (2002) Beware of density dependent pair potentials. J Phys Condens Matter 14:9187–9206
62. Warren PB (2003) Vapor-liquid coexistence in many-body dissipative particle dynamics. Phys Rev E Stat Nonlin Soft Matter Phys 68(6 Pt 2):066702. https://doi.org/10.1103/physreve.68.066702
63. Izvekov S, Rice BM (2015) On the importance of shear dissipative forces in coarse-grained dynamics of molecular liquids. Phys Chem Chem Phys 17(16):10795–10804. https://doi.org/10.1039/c4cp06116k
64. Smith GD, Bharadwaj RK (1999) Quantum chemistry based force field for simulations of HMX. J Phys Chem B 103:3570–3575
65. Choi CS, Prince E (1972) The crystal structure of cyelotrimethylene-trinitramine. Acta Crystallogr B 28:2857–2862
66. Munday LB, Chung PW, Rice BM, Solares SD (2011) Simulations of high-pressure phases in RDX. J Phys Chem B 115(15):4378–4386. https://doi.org/10.1021/jp112042a
67. Cady HH (1972) Coefficient of thermal expansion of pentaerythritol tetranitrate and hexahydro-l,3,5-trinitro-s-triazine (RDX). J Chem Eng Data 17:369–371
68. Podeszwa R, Rice BM, Szalewicz K (2009) Crystal structure prediction for cyclotrimethylene trinitramine (RDX) from first principles. Phys Chem Chem Phys 11(26):5512–5518. https://doi.org/10.1039/b902015b
69. Olinger BRB, Cady HH (1978) The linear and volume compression of B-HMX and RDX to 9 Gpa (90 Kilobar). In: Symposium International Sur Le Comportement Des Milieux Denses Sous Hautes Pressions Dynamiques, Commmissariat à l'Energie Atomique Centre d'Etudes de Vaujours Paris. France, Paris, France, pp 3–8
70. Haycraft JJ, Stevens LL, Eckhardt CJ (2006) The elastic constants and related properties of the energetic material cyclotrimethylene trinitramine (RDX) determined by Brillouin scattering. J Chem Phys 124(2):024712. https://doi.org/10.1063/1.2141958

71. Hall PG (1971) Thermal decomposition and phase transitions in solid nitramines. Trans Faraday Soc 67(578):556
72. Sellers MS, Lísal M, Brennan JK (2016) Free-energy calculations using classical molecular simulation: application to the determination of the melting point and chemical potential of a flexible RDX model. Phys Chem Chem Phys 18(11):7841–7850. https://doi.org/10.1039/c5cp06164d
73. Taylor DE (2014) Pressure dependent elastic constants of alpha and gamma cyclotrimethylene trinitramine: A quantum mechanical study. J Appl Phys 116(5):053513. https://doi.org/10.1063/1.4891999
74. Haussuhl S (2001) Elastic and thermoelastic properties of selected organic crystals: acenaphthene, trans-azobenzene, benzophenone, tolane, trans-stilbene, dibenzyl, diphenyl sulfone, 2,2'-biphenol, urea, melamine, hexogen, succinimide, pentaerythritol, urotropine, malonic acid, dimethyl malonic acid, maleic acid, hippuric acid, aluminium acetylacetonate, iron acetylacetonate, and tetraphenyl silicon. Zeitschrift für Kristallographie – Crystal Mater 216(6):339–353
75. Brennan JK, Lísal M, Moore JD, Izvekov S, Schweigert IV, Larentzos JP (2014) Coarse-grain model simulations of nonequilibrium dynamics in heterogeneous materials. J Phys Chem Lett 5(12):2144–2149. https://doi.org/10.1021/jz500756s
76. Chennamsetty N, Bock H, Lísal M, Brennan JK (2011) An introduction to coarse-graining approaches: linking atomistic and mesoscales. In: Adjiman C, Galindo A (eds) Process systems engineering, vol 6. Molecular systems engineering. WILEY-VCH Verlag GmbH & Co., KGaA, Weinheim
77. Shell MS (2016) Coarse-graining with the relative entropy. In: Rice SA, Dinner AR (eds) Advances in chemical physics, vol 161. Advances in chemical physics, pp 395–441
78. Groot RD, Stoyanov SD (2008) Mesoscopic model for colloidal particles, powders, and granular solids. Phys Rev E Stat, Nonlin Soft Matter Phys 78(5 Pt 1):051403. https://doi.org/10.1103/physreve.78.051403
79. Junghans C, Praprotnik M, Kremer K (2008) Transport properties controlled by a thermostat: an extended dissipative particle dynamics thermostat. Soft Matter 4(1):156–161. https://doi.org/10.1039/b713568h
80. Nielsen SO, Lopez CF, Srinivas G, Klein ML (2004) Coarse grain models and the computer simulation of soft materials. J Phys Condens Matter 16(15):R481–R512. https://doi.org/10.1088/0953-8984/16/15/r03
81. Depa P, Chen C, Maranas JK (2011) Why are coarse-grained force fields too fast? A look at dynamics of four coarse-grained polymers. J Chem Phys 134(1):014903. https://doi.org/10.1063/1.3513365
82. Brennan JK, Lísal M (2009) CECAM workshop: 'Dissipative particle dynamics: addressing deficiencies and establishing new frontiers' (16–18 July 2008, Lausanne, Switzerland). Mol Simul 35(9):766–769. https://doi.org/10.1080/08927020902902783
83. Venturoli M, Maddalenasperotto M, Kranenburg M, Smit B (2006) Mesoscopic models of biological membranes. Phys Rep 437(1–2):1–54. https://doi.org/10.1016/j.physrep.2006.07.006
84. Strachan A, Holian BL (2005) Energy exchange between mesoparticles and their internal degrees of freedom. Phys Rev Lett 94(1):014301. https://doi.org/10.1103/physrevlett.94.014301
85. Stoltz G (2006) A reduced model for shock and detonation waves. I. The Inert Case. Europhys Lett (EPL) 76(5):849–855. https://doi.org/10.1209/epl/i2006-10350-y
86. Maillet JB, Soulard L, Stoltz G (2007) A reduced model for shock and detonation waves. II. The Reactive Case. Europhys Lett (EPL) 78(6):68001. https://doi.org/10.1209/0295-5075/78/68001
87. Lynch K, Thompson A, Strachan A (2009) Coarse grain modeling of spall failure in molecular crystals: role of intra-molecular degrees of freedom. Modell Simul Mater Sci Eng 17(1):015007. https://doi.org/10.1088/0965-0393/17/1/015007

88. Zhou Y, Strachan A (2009) Thermal conduction in molecular materials using coarse grain dynamics: role of mass diffusion and quantum corrections for molecular dynamics simulations. J Chem Phys 131(23):234113. https://doi.org/10.1063/1.3272028
89. Brennan JK, Lísal M (2010) Coarse-grain models for metals: constant-pressure dissipative dynamics simulations. In: Proceedings of the 14th International Detonation Symposium. Office of Naval Research, ONR-351-10-185:1451-1459
90. Moore JD, Izvekov S, Lísal M, Brennan JK (2012) Particle based multiscale modeling of the dynamic response of RDX. AIP Conf Proc 1426:1237–1240. https://doi.org/10.1063/1.3686504
91. Maillet JB, Bourasseau E, Desbiens N, Vallverdu G, Stoltz G (2011) Mesoscopic simulations of shock-to-detonation transition in reactive liquid high explosive. EPL (Europhys Lett) 96(6):68007. https://doi.org/10.1209/0295-5075/96/68007
92. Lísal M, Brennan JK, Bonet Avalos J (2011) Dissipative particle dynamics at isothermal, isobaric, isoenergetic, and isoenthalpic conditions using Shardlow-like splitting algorithms. J Chem Phys 135(20):204105. https://doi.org/10.1063/1.3660209
93. Kroonblawd MP, Sewell TD, Maillet JB (2016) Characteristics of energy exchange between inter- and intramolecular degrees of freedom in crystalline 1,3,5-triamino-2,4,6-trinitrobenzene (TATB) with implications for coarse-grained simulations of shock waves in polyatomic molecular crystals. J Chem Phys 144(6):064501. https://doi.org/10.1063/1.4941332
94. Bonet Avalos J, Mackie AD (1997) Dissipative particle dynamics with energy conservation. Europhys Lett 40(2):141–146
95. Español P (1997) Dissipative particle dynamics with energy conservation. Europhys Lett 40(6):631–636
96. Mackie AD, Bonet Avalos J, Navas V (1999) Dissipative particle dynamics with energy conservation: modelling of heat flow. Phys Chem Chem Phys 1:2039–2049
97. Fogler HS (1992) Elements of Chemical Reaction Engineering. Prentice Hall, Englewood Cliffs, NJ
98. Lucy LB (1977) Numerical approach to testing of fission hypothesis. Astron J 82(12):1013–1024
99. Brenner DW, Shenderova OA, Harrison JA, Stuart SJ, Ni B, Sinnott SB (2002) A second-generation reactive empirical bond order (REBO) potential energy expression for hydrocarbons. J Phys Condensed Matter 14:783–802
100. Buckingham RA (1938) The classical equation of state of gaseous helium, neon and argon. Proc R Soc Lond A 168:264–283
101. Nikunen P, Karttunen M, Vattulainen I (2003) How would you integrate the equations of motion in dissipative particle dynamics simulations? Comput Phys Commun 153(3):407–423. https://doi.org/10.1016/s0010-4655(03)00202-9
102. Chaudhri A, Lukes JR (2010) Velocity and stress autocorrelation decay in isothermal dissipative particle dynamics. Phys Rev E Stat, Nonlin Soft Matter Phys 81(2 Pt 2):026707. https://doi.org/10.1103/physreve.81.026707
103. Vattulainen I, Karttunen M, Besold G, Polson JM (2002) Integration schemes for dissipative particle dynamics simulations: from softly interacting systems towards hybrid models. J Chem Phys 116(10):3967–3979. https://doi.org/10.1063/1.1450554
104. Larentzos JP, Brennan JK, Moore JD, Lísal M, Mattson WD (2014) Parallel implementation of isothermal and isoenergetic dissipative particle dynamics using shardlow-like splitting algorithms. Comput Phys Commun 185(7):1987–1998. https://doi.org/10.1016/j.cpc.2014.03.029
105. Homman AA, Maillet JB, Roussel J, Stoltz G (2016) New parallelizable schemes for integrating the dissipative particle dynamics with energy conservation. J Chem Phys 144(2):024112. https://doi.org/10.1063/1.4937797
106. Stoltz G (2017) Stable schemes for dissipative particle dynamics with conserved energy. J Comput Phys 340:451–469. https://doi.org/10.1016/j.jcp.2017.03.059

107. Shardlow T (2003) Splitting for dissipative particle dynamics. SIAM J Sci Comput 24(4):1267–1282
108. Plimpton SJ (1995) Fast parallel algorithms for short-range molecular dynamics. J Comput Phys 117:1–19
109. Senftle TP, Hong S, Islam MM, Kylasa SB, Zheng Y, Shin YK, Junkermeier C, Engel-Herbert R, Janik MJ, Aktulga HM, Verstraelen T, Grama A, van Duin ACT (2016) The ReaxFF reactive force-field: development, applications and future directions. npj Comput Mater 2:15011. https://doi.org/10.1038/npjcompumats.2015.11
110. Shan TR, van Duin AC, Thompson AP (2014) Development of a ReaxFF reactive force field for ammonium nitrate and application to shock compression and thermal decomposition. J Phys Chem A 118(8):1469–1478. https://doi.org/10.1021/jp408397n
111. Mathew N, Picu RC (2011) Molecular conformational stability in cyclotrimethylene trinitramine crystals. J Chem Phys 135(2):024510. https://doi.org/10.1063/1.3609769
112. Broadbelt LJ, Pfaendtner J (2005) Lexicography of kinetic modeling of complex reaction networks. AlChE J 51(8):2112–2121. https://doi.org/10.1002/aic.10599
113. Klippenstein SJ (2017) From theoretical reaction dynamics to chemical modeling of combustion. Proc Combust Inst 36(1):77–111. https://doi.org/10.1016/j.proci.2016.07.100
114. Yetter Rad FL, Allen MT, Gatto JL (1995) Development of gas-phase reaction mechanisms for nitramine combustion. J Propul Power 11(4):683–697
115. Kumbhakarna N, Thynell ST, Chowdhury A, Lin P (2011) Analysis of RDX-TAGzT pseudo-propellant combustion with detailed chemical kinetics. Combust Theor Model 15(6):933–956. https://doi.org/10.1080/13647830.2011.591503
116. Taylor DE, Rice BM (2014) Quantum-informed multiscale M&S for energetic materials. In: Sabin JR (ed) Advances in quantum chemistry: energetic materials, vol 69. Academic Press. Cambridge, MA, pp 171–204
117. Manaa MR, Fried LE (2014) The reactivity of energetic materials under high pressure and temperature. In: Sabin JR (ed) Advances in quantum chemistry: energetic materials, vol 69. Academic Press, Cambridge, MA, pp 221–252. https://doi.org/10.1016/b978-0-12-800345-9.00006-4
118. Reed EJ, Riad Manaa M, Fried LE, Glaesemann KR, Joannopoulos JD (2007) A transient semimetallic layer in detonating nitromethane. Nat Phys 4(1):72–76. https://doi.org/10.1038/nphys806
119. Manaa MR, Reed EJ, Fried LE, Goldman N (2009) Nitrogen-rich heterocycles as reactivity retardants in shocked insensitive explosives. J Am Chem Soc 131:5483–5487
120. Manaa MR, Fried LE, Melius CF, Elstner M, Frauenheim T (2002) Decomposition of HMX at extreme conditions: a molecular dynamics simulation. J Phys Chem A 106:9024–9029
121. Ge NN, Wei YK, Ji GF, Chen XR, Zhao F, Wei DQ (2012) Initial decomposition of the condensed-phase beta-HMX under shock waves: molecular dynamics simulations. J Phys Chem B 116(46):13696–13704. https://doi.org/10.1021/jp309120t
122. Zhu W, Huang H, Huang H, Xiao H (2012) Initial chemical events in shocked octahydro-1,3,5,7-tetranitro-1,3,5,7-tetrazocine: a new initiation decomposition mechanism. J Chem Phys 136(4):044516. https://doi.org/10.1063/1.3679384
123. Ge NN, Wei YK, Zhao F, Chen XR, Ji GF (2014) Pressure-induced metallization of condensed phase beta-HMX under shock loadings via molecular dynamics simulations in conjunction with multi-scale shock technique. J Mol Model 20(7):2350. https://doi.org/10.1007/s00894-014-2350-1
124. Reed EJ, Rodriguez AW, Manaa MR, Fried LE, Tarver CM (2012) Ultrafast detonation of hydrazoic acid (HN3). Phys Rev Lett 109(3):038301. https://doi.org/10.1103/physrevlett.109.038301
125. Manaa MR, Fried LE, Reed EJ (2003) Explosive chemistry: Simulating the chemistry of energetic materials at extreme conditions. J Comput Aided Mater Des 10(2):75–97. https://doi.org/10.1023/b:jcad.0000036812.64349.15
126. An Q, Liu W-G, Goddard WA, Cheng T, Zybin SV, Xiao H (2014) Initial steps of thermal decomposition of dihydroxylammonium 5,5′-bistetrazole-1,1′-diolate crystals from quantum mechanics. J Phys Chem C 118(46):27175–27181. https://doi.org/10.1021/jp509582x

127. Wu Q, Xiang D, Xiong G, Zhu W, Xiao H (2016) Coupling of temperature with pressure induced initial decomposition mechanisms of two molecular crystals: an ab initio molecular dynamics study. J Chem Sci 128(5):695–705. https://doi.org/10.1007/s12039-016-1068-2
128. Wu Q, Zhu W, Xiao H (2016) Cooperative effects of different temperatures and pressures on the initial and subsequent decomposition reactions of the nitrogen-rich energetic crystal 3,3′-dinitroamino-4,4′-azoxyfurazan. Phys Chem Chem Phys 18(10):7093–7099. https://doi.org/10.1039/c6cp00096g
129. Wu Q, Chen H, Xiong G, Zhu W, Xiao H (2015) Decomposition of a 1,3,5-triamino-2,4,6-trinitrobenzene crystal at decomposition temperature coupled with different pressures: an ab initio molecular dynamics study. J Phys Chem C 119(29):16500–16506. https://doi.org/10.1021/acs.jpcc.5b05041
130. Ye C-C, An Q, Cheng T, Zybin S, Naserifar S, Ju X-H, Goddard III WA (2015) Reaction mechanism from quantum molecular dynamics for the initial thermal decomposition of 2,4,6-triamino-1,3,5-triazine-1,3,5-trioxide (MTO) and 2,4,6-trinitro-1,3,5-triazine-1,3,5-trioxide (MTO3 N), promising green energetic materials. J Mater Chem A 3(22):12044–12050. https://doi.org/10.1039/c5ta02486b
131. Ye C-C, An Q, Goddard III WA, Cheng T, Liu W-G, Zybin SV, Ju X-H (2015) Initial decomposition reaction of di-tetrazine-tetroxide (DTTO) from quantum molecular dynamics: implications for a promising energetic material. J Mater Chem A 3(5):1972–1978. https://doi.org/10.1039/c4ta05676k
132. Ge NN, Wei YK, Song ZF, Chen XR, Ji GF, Zhao F, Wei DQ (2014) Anisotropic responses and initial decomposition of condensed-phase beta-HMX under shock loadings via molecular dynamics simulations in conjunction with multiscale shock technique. J Phys Chem B 118(29):8691–8699. https://doi.org/10.1021/jp502432g
133. He ZH, Chen J, Wu Q, Ji GF (2016) Special catalytic effects of intermediate-water for rapid shock initiation of beta-HMX. RSC Adv 6(95):93103–93110. https://doi.org/10.1039/c6ra21384g
134. Wu Q, Xiong G, Zhu W, Xiao H (2015) How does low temperature coupled with different pressures affect initiation mechanisms and subsequent decompositions in nitramine explosive HMX? Phys Chem Chem Phys 17(35):22823–22831. https://doi.org/10.1039/c5cp03257a
135. Xue X, Wen Y, Zhang C (2016) Early decay mechanism of shocked ε-CL-20: a molecular dynamics simulation study. J Phys Chem C 120(38):21169–21177. https://doi.org/10.1021/acs.jpcc.6b05228
136. He ZH, Chen J, Ji GF, Liu LM, Zhu WJ, Wu Q (2015) Dynamic responses and initial decomposition under shock loading: A DFTB calculation combined with MSST method for beta-HMX with molecular vacancy. J Phys Chem B 119(33):10673–10681. https://doi.org/10.1021/acs.jpcb.5b05081
137. Joshi KL, Chaudhuri S (2015) Reactive simulation of the chemistry behind the condensed-phase ignition of RDX from hot spots. Phys Chem Chem Phys 17(28):18790–18801. https://doi.org/10.1039/c5cp00950b
138. Furman D, Kosloff R, Zeiri Y (2016) Effects of nanoscale heterogeneities on the reactivity of shocked erythritol tetranitrate. J Phys Chem C 120(50):28886–28893. https://doi.org/10.1021/acs.jpcc.6b11543
139. Zhou T, Lou J, Zhang Y, Song H, Huang F (2016) Hot spot formation and chemical reaction initiation in shocked HMX crystals with nanovoids: a large-scale reactive molecular dynamics study. Phys Chem Chem Phys 18(26):17627–17645. https://doi.org/10.1039/c6cp02015a
140. Wen Y, Xue X, Long X, Zhang C (2016) Cluster evolution at early stages of 1,3,5-triamino-2,4,6-trinitrobenzene under various heating conditions: a molecular reactive force field study. J Phys Chem A 120(22):3929–3937. https://doi.org/10.1021/acs.jpca.6b03795
141. Yu Y, Chen S, Li X, Zhu J, Liang H, Zhang X, Shu Q (2016) Molecular dynamics simulations for 5,5′-bistetrazole-1,1′-diolate (TKX-50) and its PBXs. RSC Adv 6(24):20034–20041. https://doi.org/10.1039/c5ra27912g
142. Wood MA, Strachan A (2016) Nonequilibrium reaction kinetics in molecular solids. J Phys Chem C 120(1):542–552. https://doi.org/10.1021/acs.jpcc.5b09820

143. Guo D, Zybin SV, An Q, Goddard III WA, Huang F (2016) Prediction of the Chapman-Jouguet chemical equilibrium state in a detonation wave from first principles based reactive molecular dynamics. Phys Chem Chem Phys 18(3):2015–2022. https://doi.org/10.1039/c5cp04516a
144. Wood MA, Cherukara MJ, Kober EM, Strachan A (2015) Ultrafast chemistry under nonequilibrium conditions and the shock to deflagration transition at the nanoscale. J Phys Chem C 119(38):22008–22015. https://doi.org/10.1021/acs.jpcc.5b05362
145. Xue X, Wen Y, Long X, Li J, Zhang C (2015) Influence of dislocations on the shock sensitivity of RDX: molecular dynamics simulations by reactive force field. J Phys Chem C 119(24):13735–13742. https://doi.org/10.1021/acs.jpcc.5b03298
146. Wen Y, Zhang C, Xue X, Long X (2015) Cluster evolution during the early stages of heating explosives and its relationship to sensitivity: a comparative study of TATB, beta-HMX and PETN by molecular reactive force field simulations. Phys Chem Chem Phys 17(18):12013–12022. https://doi.org/10.1039/c5cp00006h
147. Zhou TT, Lou JF, Song HJ, Huang FL (2015) Anisotropic shock sensitivity in a single crystal delta-cyclotetramethylene tetranitramine: a reactive molecular dynamics study. Phys Chem Chem Phys 17(12):7924–7935. https://doi.org/10.1039/c4cp05575f
148. Guo D, An Q, Zybin SV, Goddard III WA, Huang F, Tang B (2015) The co-crystal of TNT/CL-20 leads to decreased sensitivity toward thermal decomposition from first principles based reactive molecular dynamics. J Mater Chem A 3(10):5409–5419. https://doi.org/10.1039/c4ta06858k
149. Guo D, An Q, Goddard WA, Zybin SV, Huang F (2014) Compressive shear reactive molecular dynamics studies indicating that cocrystals of TNT/CL-20 decrease sensitivity. J Phys Chem C 118(51):30202–30208. https://doi.org/10.1021/jp5093527
150. Li Y, Kalia RK, Nakano A, K-I Nomura, Vashishta P (2014) Multistage reaction pathways in detonating high explosives. Appl Phys Lett 105(20):204103. https://doi.org/10.1063/1.4902128
151. Zhou T, Liu L, Goddard WA 3rd, Zybin SV, Huang F (2014) ReaxFF reactive molecular dynamics on silicon pentaerythritol tetranitrate crystal validates the mechanism for the colossal sensitivity. Phys Chem Chem Phys 16(43):23779–23791. https://doi.org/10.1039/c4cp03781b
152. An Q, Goddard WA, Zybin SV, Luo S-N (2014) Inhibition of hotspot formation in polymer bonded explosives using an interface matching low density polymer coating at the polymer-explosive interface. J Phys Chem C 118(34):19918–19928. https://doi.org/10.1021/jp506501r
153. Zhou T, Song H, Liu Y, Huang F (2014) Shock initiated thermal and chemical responses of HMX crystal from ReaxFF molecular dynamics simulation. Phys Chem Chem Phys 16(27):13914–13931. https://doi.org/10.1039/c4cp00890a
154. Wu CJ, Fried LE, Yang LH, Goldman N, Bastea S (2009) Catalytic behaviour of dense hot water. Nat Chem 1(1):57–62. https://doi.org/10.1038/nchem.130
155. Rice BM, Byrd EF (2016) Theoretical study of shocked formic acid: Born-Oppenheimer MD calculations of the shock Hugoniot and early-stage chemistry. J Phys Chem B 120(8):1711–1719. https://doi.org/10.1021/acs.jpcb.5b08845
156. van Duin AC, Zeiri Y, Dubnikova F, Kosloff R, Goddard III WA (2005) Atomistic-scale simulations of the initial chemical events in the thermal initiation of triacetonetriperoxide. J Am Chem Soc 127:11053–11062
157. Reed EJ, Fried LE, Joannopoulos JD (2003) A method for tractable dynamical studies of single and double shock compression. Phys Rev Lett 90(23):235503. https://doi.org/10.1103/physrevlett.90.235503
158. Reed EJF, Laurence E, Manaa, MR., Joannopoulos JD (2005) A multi-scale approach to molecular dynamics simulations of shock waves. In: Manaa MR (ed) Chemistry at extreme conditions. Elsevier B.V., Amsterdam, Neth, pp 297–325. https://doi.org/10.1016/b978-044451766-1/50010-x
159. Goldman N, Reed EJ, Fried LE (2009) Quantum mechanical corrections to simulated shock Hugoniot temperatures. J Chem Phys 131(20):204103. https://doi.org/10.1063/1.3262710

160. Qi T, Reed EJ (2012) Simulations of shocked methane including self-consistent semiclassical quantum nuclear effects. J Phys Chem A 116(42):10451–10459. https://doi.org/10.1021/jp308068c
161. Elstner M, Porezag D, Jungnickel G, Elsner J, Haugk M, Frauenheim T, Suhai S, Seifert G (1998) Self-consistent-charge density-functional tight-binding method for simulations of complex materials properties. Phys Rev B 58:7260
162. Maillet JB, Bourasseau E (2009) ab initio simulations of thermodynamic and chemical properties of detonation product mixtures. J Chem Phys 131(8):084107. https://doi.org/10.1063/1.3179671
163. Cawkwell MJ, Niklasson AM, Dattelbaum DM (2015) Extended Lagrangian Born-Oppenheimer molecular dynamics simulations of the shock-induced chemistry of phenylacetylene. J Chem Phys 142(6):064512. https://doi.org/10.1063/1.4907909
164. Reed EJ (2012) Electron-ion coupling in shocked energetic materials. J Phys Chem C 116(3):2205–2211. https://doi.org/10.1021/jp206769c
165. Tarver CM, Forbes JW, Urtiew PA (2007) Nonequilibrium Zeldovich-von Neumann-Doring theory and reactive flow modeling of detonation. Russian J Phys Chem B 1(1):39–45. https://doi.org/10.1134/s1990793107010058
166. Reed DA, Dongarra J (2015) Exascale computing and big data. Commun ACM 58(7):56–68. https://doi.org/10.1145/2699414
167. Dongarra J, Beckman P, Moore T, Aerts P, Aloisio G, Andre JC, Barkai D, Berthou JY, Boku T, Braunschweig B, Cappello F, Chapman B, Xuebin C, Choudhary A, Dosanjh S, Dunning T, Fiore S, Geist A, Gropp B, Harrison R, Hereld M, Heroux M, Hoisie A, Hotta K, Zhong J, Ishikawa Y, Johnson F, Kale S, Kenway R, Keyes D, Kramer B, Labarta J, Lichnewsky A, Lippert T, Lucas B, Maccabe B, Matsuoka S, Messina P, Michielse P, Mohr B, Mueller MS, Nagel WE, Nakashima H, Papka ME, Reed D, Sato M, Seidel E, Shalf J, Skinner D, Snir M, Sterling T, Stevens R, Streitz F, Sugar B, Sumimoto S, Tang W, Taylor J, Thakur R, Trefethen A, Valero M, van der Steen A, Vetter J, Williams P, Wisniewski R, Yelick K (2011) The international exascale software project roadmap. Int J High Perform Comput Appl 25(1):3–60. https://doi.org/10.1177/1094342010391989
168. Geist A, Reed DA (2017) A survey of high-performance computing scaling challenges. Int J High Perf Comput Appl 31(1):104–113. https://doi.org/10.1177/1094342015597083
169. Li Z, Kermode JR, De Vita A (2015) Molecular dynamics with on-the-fly machine learning of quantum-mechanical forces. Phys Rev Lett 114(9):096405. https://doi.org/10.1103/physrevlett.114.096405
170. Kalidindi SR, De Graef M (2015) Materials data science: current status and future outlook. Annual Rev Mater Res 45(1):171–193. https://doi.org/10.1146/annurev-matsci-070214-020844
171. Matouš K, Geers MGD, Kouznetsova VG, Gillman A (2017) A review of predictive nonlinear theories for multiscale modeling of heterogeneous materials. J Comput Phys 330:192–220. https://doi.org/10.1016/j.jcp.2016.10.070
172. Coveney PV, Dougherty ER, Highfield RR (2016) Big data need big theory too. Philos Trans A Math Phys Eng Sci 374(2080). https://doi.org/10.1098/rsta.2016.0153
173. Pham TL, Kino H, Terakura K, Miyake T, Dam HC (2016) Novel mixture model for the representation of potential energy surfaces. J Chem Phys 145(15):154103. https://doi.org/10.1063/1.4964318
174. Geiger P, Dellago C (2013) Neural networks for local structure detection in polymorphic systems. J Chem Phys 139(16):164105. https://doi.org/10.1063/1.4825111
175. Lee K, Joshi K, Chaudhuri S, Stewart DS (2016) Mirrored continuum and molecular scale simulations of the ignition of high-pressure phases of RDX. J Chem Phys 144(18):184111. https://doi.org/10.1063/1.4948548
176. Cawkwell MJ, Luscher DJ, Addessio FL, Ramos KJ (2016) Equations of state for the α and γ polymorphs of cyclotrimethylene trinitramine. J Appl Phys 119(18):185106. https://doi.org/10.1063/1.4948673

177. Sewell TD, Bennett CM (2000) Monte Carlo calculations of the elastic moduli and pressure-volume-temperature equation of state for hexahydro-1,3,5-trinitro-1,3,5-triazine. J Appl Phys 88(1):88
178. Larentzos JP, Rice BM (2017) Transferable reactive force fields: extensions of ReaxFF-lg to nitromethane. J Phys Chem A 121(9):2001–2013. https://doi.org/10.1021/acs.jpca.6b11761
179. Park HS, Karpov EG, Liu† WK, Klein PA (2005) The bridging scale for two-dimensional atomistic/continuum coupling. Philos Mag 85(1):79–113. https://doi.org/10.1080/14786430412331300163
180. Roehm D, Pavel RS, Barros K, Rouet-Leduc B, McPherson AL, Germann TC, Junghans C (2015) Distributed database kriging for adaptive sampling. Comput Phys Commun 192:138–147. https://doi.org/10.1016/j.cpc.2015.03.006
181. Miller RE, Tadmor EB (2009) A unified framework and performance benchmark of fourteen multiscale atomistic/continuum coupling methods. Model Simul Mater Sci Eng 17(5):053001. https://doi.org/10.1088/0965-0393/17/5/053001
182. Stjernschantz E, Marelius J, Medina C, Jacobsson M, Vermeulen NPE, Oostenbrink C (2006) Are automated molecular dynamics simulations and binding free energy calculations realistic tools in lead optimization? An evaluation of the linear interaction energy (LIE) method. J Chem Inf Model 46:1972–1983
183. Tang Y-H, Kudo S, Bian X, Li Z, Karniadakis GE (2015) Multiscale universal interface: a concurrent framework for coupling heterogeneous solvers. J Comput Phys 297:13–31. https://doi.org/10.1016/j.jcp.2015.05.004
184. Kevrekidis IG, Samaey G (2009) Equation-free multiscale computation: algorithms and applications. Annual Rev Phys Chem 60:321–344. https://doi.org/10.1146/annurev.physchem.59.032607.093610
185. Bunder JE, Roberts AJ, Kevrekidis IG (2017) Good coupling for the multiscale patch scheme on systems with microscale heterogeneity. J Comput Phys 337:154–174. https://doi.org/10.1016/j.jcp.2017.02.004
186. Barton NR, Bernier JV, Knap J, Sunwoo AJ, Cerreta EK, Turner TJ (2011) A call to arms for task parallelism in multi-scale materials modeling. Int J Numer Meth Engng 86(6):744–764. https://doi.org/10.1002/nme.3071
187. Kouznetsova V, Geers MGD, Brekelmans WAM (2002) Multi-scale constitutive modelling of heterogeneous materials with a gradient-enhanced computational homogenization scheme. Int J Numer Meth Eng 54(8):1235–1260. https://doi.org/10.1002/nme.541
188. Özdemir I, Brekelmans WAM, Geers MGD (2008) Computational homogenization for the thermo-mechanical analysis of heterogeneous solids. Comput Methods Appl Mech Engrg 198(3–4):602–613. https://doi.org/10.1016/j.cma.2008.09.008
189. Weinan E, Engquist B, Li X, Ren W, Vanden-Eijnden E (2007) Heterogeneous multiscale methods: a review. Commun Comput Phys 2(3):367–450
190. Abdulle A, Weinan E, Engquist B, Vanden-Eijnden E (2012) The heterogeneous multiscale method. Acta Numer 21:1–87. https://doi.org/10.1017/s0962492912000025
191. Wescott BL, Stewart DS, Davis WC (2005) Equation of state and reaction rate for condensed-phase explosives. J Appl Phys 98(5):053514. https://doi.org/10.1063/1.2035310
192. Myint PC, McClelland MA, Nichols AL (2016) Application of the Peng–Robinson equation of state to energetic materials RDX and TNT: pure components, liquid mixtures, and solid mixtures. Industr Eng Chem Res 55(7):2252–2266. https://doi.org/10.1021/acs.iecr.5b04808
193. Cooper PW (1998) Introduction to detonation physics. In: Zukas JA (ed) Explosive effects and applications
194. Lee EL, Tarver CM (1980) Phenomenological model of shock initiation in heterogeneous explosives. Phys Fluids 23(12):2362. https://doi.org/10.1063/1.862940
195. Bastea S, Fried LE (2012) Chemical equilibrium detonation. In: Zhang F (ed) Shock wave science and technology reference library, vol 6. https://doi.org/10.1007/978-3-642-22967-1
196. Henson BF (2002) Ignition chemistry in HMX from thermal explosion to detonation, 620:1069–1072. https://doi.org/10.1063/1.1483723

197. Reaugh JE (2011) HERMES: a model to describe deformation, burning, explosion, and detonation. Technical Report LLNL-TR-516119, Lawrence Livermore National Laboratory
198. Rice BM (2017) A perspective on modeling the multiscale response of energetic materials. AIP Conf Proc 1793:020003. https://doi.org/10.1063/1.4971458
199. Nichols III AL (2007) ALE-3D user's manual. Technical report UCRL-MA-152204, Lawrence Livermore National Laboratory
200. Knap J, Barton NR, Hornung RD, Arsenlis A, Becker R, Jefferson DR (2008) Adaptive sampling in hierarchical simulation. Int J Numer Meth Eng 76(4):572–600. https://doi.org/10.1002/nme.2339
201. Knap J, Spear C, Leiter K, Becker R, Powell D (2016) A computational framework for scale-bridging in multi-scale simulations. Int J Numer Meth Engng 108:1649–1666. https://doi.org/10.1002/nme.5270
202. Schmidt MG, Ismail AE, Sauer RA (2015) A continuum mechanical surrogate model for atomic beam structures. J Multiscale Comp Engrg 13(5):413–442
203. Wirtz D, Karajan N, Haasdonk B (2015) Surrogate modeling of multiscale models using kernel methods. Int J Numer Meth Eng 101(1):1–28. https://doi.org/10.1002/nme.4767
204. Balachandran PV, Xue D, Theiler J, Hogden J, Lookman T (2016) Adaptive strategies for materials design using uncertainties. Sci Rep 6:19660. https://doi.org/10.1038/srep19660
205. Rouet-Leduc B, Barros K, Cieren E, Elango V, Junghans C, Lookman T, Mohd-Yusof J, Pavel RS, Rivera AY, Roehm D, McPherson AL, Germann TC (2014) Spatial adaptive sampling in multiscale simulation. Comput Phys Commun 185(7):1857–1864. https://doi.org/10.1016/j.cpc.2014.03.011
206. Behler J (2016) Perspective: machine learning potentials for atomistic simulations. J Chem Phys 145(17):170901. https://doi.org/10.1063/1.4966192
207. Ling J, Jones R, Templeton J (2016) Machine learning strategies for systems with invariance properties. J Comput Phys 318:22–35. https://doi.org/10.1016/j.jcp.2016.05.003
208. Pilania G, Gubernatis JE, Lookman T (2017) Multi-fidelity machine learning models for accurate bandgap predictions of solids. Comp Mater Sci 129:156–163. https://doi.org/10.1016/j.commatsci.2016.12.004
209. Ramakrishnan R, Dral PO, Rupp M, von Lilienfeld OA (2015) Big data meets quantum chemistry approximations: the delta-machine learning approach. J Chem Theory Comput 11(5):2087–2096. https://doi.org/10.1021/acs.jctc.5b00099
210. Barnes BC, Leiter KW, Becker R, Knap J, Brennan JK (2017) LAMMPS integrated materials engine (LIME) for efficient automation of particle-based simulations: application to equation of state generation. Modell Simul Mater Sci Eng 25(5):055006. https://doi.org/10.1088/1361-651x/aa6e36
211. Feng Y (2017) Python-mpi-bcast. https://github.com/rainwoodman/python-mpi-bcast. Accessed 22 Mar 2017
212. Fried LE (2007) The reactivity of energetic materials at extreme conditions. In: Lipkowitz KBC, Cundari TR (ed) Reviews in computational chemistry, vol 25. Wiley Inc., Hoboken, NJ, pp 159–189. https://doi.org/10.1002/9780470189078.ch4
213. Tarver CM (2006) Detonation reaction zones in condensed explosives. AIP Conf Proc 845:1026–1029. https://doi.org/10.1063/1.2263497
214. Johnson JN, Tang PK, Forest CA (1985) Shock-wave initiation of heterogeneous reactive solids. J Appl Phys 57(9):4323. https://doi.org/10.1063/1.334591
215. Rimoli JJ, Gürses E, Ortiz M (2010) Shock-induced subgrain microstructures as possible homogenous sources of hot spots and initiation sites in energetic polycrystals. Phys Rev B 81(1). https://doi.org/10.1103/physrevb.81.014112
216. An Q, Zybin SV, Goddard WA, Jaramillo-Botero A, Blanco M, Luo S-N (2011) Elucidation of the dynamics for hot-spot initiation at nonuniform interfaces of highly shocked materials. Phys Rev B 84(22). https://doi.org/10.1103/physrevb.84.220101
217. Todd SN, Caipen TL, Anderson MU, Lee BD (2011) Modeling damage induced initiation of explosives. Exp Mech 52(2):145–151. https://doi.org/10.1007/s11340-011-9533-9

218. Tsyshevsky RV, Sharia O, Kuklja MM (2016) Molecular theory of detonation initiation: insight from first principles modeling of the decomposition mechanisms of organic nitro energetic materials. Molecules 21(2). https://doi.org/10.3390/molecules21020236
219. Bdzil JB, Stewart DS (2007) The dynamics of detonation in explosive systems*. Annual Rev Fluid Mech 39(1):263–292. https://doi.org/10.1146/annurev.fluid.38.050304.092049
220. Baer MR, Gartling DK, DesJardin PE (2012) Probabilistic models for reactive behaviour in heterogeneous condensed phase media. Combust Theor Model 16(1):75–106. https://doi.org/10.1080/13647830.2011.606916
221. Ostoja-Starzewski M, Wang X (1999) Stochastic finite elements as a bridge between random material microstructure and global response. Comput Methods Appl Mech Eng 169:35–49
222. Ostoja-Starzewski M (2006) Material spatial randomness: from statistical to representative volume element. Probab Eng Mech 21(2):112–132. https://doi.org/10.1016/j.probengmech.2005.07.007
223. Yin X, Chen W, To A, McVeigh C, Liu WK (2008) Statistical volume element method for predicting microstructure–constitutive property relations. Comput Methods Appl Mech Engrg 197(43–44):3516–3529. https://doi.org/10.1016/j.cma.2008.01.008
224. Qidwai SM, Turner DM, Niezgoda SR, Lewis AC, Geltmacher AB, Rowenhorst DJ, Kalidindi SR (2012) Estimating the response of polycrystalline materials using sets of weighted statistical volume elements. Acta Mater 60(13–14):5284–5299. https://doi.org/10.1016/j.actamat.2012.06.026
225. Tripathy R, Bilionis I, Gonzalez M (2016) Gaussian processes with built-in dimensionality reduction: applications to high-dimensional uncertainty propagation. J Comput Phys 321:191–223. https://doi.org/10.1016/j.jcp.2016.05.039
226. Breiman L (2001) Statistical modeling: the two cultures. Stat Sci 16(3):199–231
227. Weirs VG, Kamm JR, Swiler LP, Tarantola S, Ratto M, Adams BM, Rider WJ, Eldred MS (2012) Sensitivity analysis techniques applied to a system of hyperbolic conservation laws. Reliab Eng Syst Safety 107:157–170. https://doi.org/10.1016/j.ress.2011.12.008
228. Sen O, Davis S, Jacobs G, Udaykumar HS (2015) Evaluation of convergence behavior of metamodeling techniques for bridging scales in multi-scale multimaterial simulation. J Comput Phys 294:585–604. https://doi.org/10.1016/j.jcp.2015.03.043
229. Bhattacharjee S, Matouš K (2016) A nonlinear manifold-based reduced order model for multiscale analysis of heterogeneous hyperelastic materials. J Comput Phys 313:635–653. https://doi.org/10.1016/j.jcp.2016.01.040